

# Atom-dimer and dimer-dimer scattering in fermionic mixtures near a narrow Feshbach resonance

J. Levinsen<sup>1,2</sup> and D. S. Petrov<sup>2,3</sup>

<sup>1</sup> T.C.M. Group, University of Cambridge, Cavendish Laboratory, J. J. Thomson Ave., Cambridge CB3 0HE, United Kingdom

<sup>2</sup> Laboratoire de Physique Théorique et Modèles Statistiques, CNRS and Université Paris Sud, UMR8626, Bât. 100, 91405 Orsay, France

<sup>3</sup> Russian Research Center Kurchatov Institute, Kurchatov Square, 123182 Moscow, Russia

Received: date / Revised version: date

**Abstract.** We develop a diagrammatic approach for solving few-body problems in heteronuclear fermionic mixtures near a narrow interspecies Feshbach resonance. We calculate *s*-, *p*-, and *d*-wave phaseshifts for the scattering of an atom by a weakly-bound dimer. The fermionic statistics of atoms and the composite nature of the dimer lead to a strong angular momentum dependence of the atom-dimer interaction, which manifests itself in a peculiar interference of the scattered *s*- and *p*-waves. This effect strengthens with the mass ratio and is remarkably pronounced in  $^{40}\text{K}$ - $(^{40}\text{K}-^6\text{Li})$  atom-dimer collisions. We calculate the scattering length for two dimers formed near a narrow interspecies resonance. Finally, we discuss the collisional relaxation of the dimers to deeply bound states and evaluate the corresponding rate constant as a function of the detuning and collision energy.

**PACS.** XX.XX.XX No PACS code given

## 1 Introduction

Numerous advances in the field of ultracold Fermi gases over the past decade have enabled the exploration of novel strongly interacting regimes in fermionic systems (see [1] and [2] for review). The BCS-BEC crossover, extensively studied in either Potassium ( $^{40}\text{K}$ ) or Lithium ( $^6\text{Li}$ ) homonuclear systems, is now being actively pursued in the new generation of experiments on mixtures of these two isotopes [3–10]. The mass ratio is thus a new parameter introduced into the crossover phase diagram [11]. It is then natural to ask whether changing this parameter can lead to qualitatively new crossover physics and, if so, how large should the mass ratio be in order to see non-trivial effects?

For a very large mass ratio (of the order of several hundreds) a crystalline phase can emerge on the BEC side of the crossover [12]. The effect is due to a strong long-range repulsion between the heavy fermions originating from the exchange of their light partners. Another mass ratio dependent change in the behavior of the system occurs in the problem of two identical heavy fermions of mass  $m_\uparrow$  interacting resonantly with a light atom of mass  $m_\downarrow$ . The exchange of the light atom results in an attractive potential between the heavy fermions proportional to  $1/m_\downarrow R^2$ , where  $R$  is the distance between them. This exchange attraction competes with the repulsive centrifugal barrier  $\propto 1/m_\uparrow R^2$  for the identical fermions. For mass ratios  $m_\uparrow/m_\downarrow$  larger than the critical value 13.6 the exchange attraction dominates over the centrifugal barrier and the

heavy particles experience a fall to the centre in the  $1/R^2$ -potential [13]. On resonance (interspecies scattering length  $a = \infty$ ) this leads to the Efimov effect - the existence of an infinite number of bound heavy-heavy-light trimer states [14–16]. For smaller mass ratios the centrifugal barrier is dominant. On the one hand this effective three-body repulsion excludes the Efimov effect. On the other it suppresses recombination processes requiring three atoms to approach each other to very short distances, which is evidently advantageous for the collisional stability of the gas. The lower the mass ratio, the more stable this three-body system is [17].

It turns out that even for  $m_\uparrow/m_\downarrow < 13.6$  the  $\uparrow\uparrow\downarrow$ -system exhibits non-perturbative effects on the positive (BEC) side of the resonance, where there is a weakly bound heteronuclear molecular state. One of us found that the three-body recombination to this state vanishes for  $m_\uparrow/m_\downarrow \approx 8.6$  [18]. Later, Kartavtsev and Malykh argued that this phenomenon is related to the existence of a weakly bound *not* Efimovian trimer state for  $m_\uparrow/m_\downarrow > 8.2$  [19]. The trimer has unit angular momentum and for smaller mass ratios turns into a *p*-wave atom-dimer scattering resonance. We have recently shown that in the case of a K-Li mixture ( $m_\uparrow/m_\downarrow = 6.64$ ) the K-(K-Li) atom-dimer scattering should be dominated by this *p*-wave resonance in a wide range of collision energies [20]. Moreover, by introducing an external quasi-2D confinement, the *p*-wave atom-dimer interaction can be tuned from attractive to repulsive, allowing for a trimer formation.

In this paper we develop a uniform-space diagrammatic approach for studying few-body processes in a heteronuclear fermionic mixture near an interspecies Feshbach resonance of finite width. We calculate relevant atom-dimer scattering phaseshifts and partial cross-sections in the homonuclear case and in the K-Li case. Passing from  $m_\uparrow/m_\downarrow = 1$  to  $m_\uparrow/m_\downarrow = 6.64$  we observe an increase in the atom-dimer interaction, repulsive in even angular momentum channels and attractive in odd ones. The most dramatic increase is found in the channel with unit angular momentum – the  $p$ -wave scattering volume changes by more than an order of magnitude. Our exact calculations are complemented by a qualitative explanation of the observed effect based on the Born-Oppenheimer approach, which we generalize to the case of a narrow interspecies resonance. We predict a very strong interference between  $s$ - and  $p$ -waves in atom-dimer scattering. Depending on the collision energy, the scattering is dominant in backward or forward directions, which can be observed experimentally by colliding an atomic cloud with a cloud of molecules. We use our diagrammatic approach to calculate the dimer-dimer scattering length  $a_{dd}$  as a function of the atomic scattering length  $a$  and the width of the interspecies resonance. Finally, we discuss the main mechanisms of the collisional relaxation of dimers into deep molecular states, and calculate the corresponding atom-dimer and dimer-dimer relaxation rate constants as functions of  $a$ , the width of the resonance, and the collision energy.

The paper is organized as follows. In Sec. 2 we discuss the two-body problem in the narrow resonance case and introduce our field-theoretical approach. The main part of the paper is structured according to the previous paragraph – Secs. 3 and 4 are devoted to the three- and four-body problems respectively. In Sec. 5 we discuss the inelastic collisional relaxation in atom-dimer and dimer-dimer collisions, and in Sec. 6 we conclude.

## 2 Two-body problem near a narrow Feshbach resonance

We assume that all interatomic interactions in the  $\uparrow\downarrow$  fermionic mixture are characterized by van der Waals potentials. We also assume that the intraspecies interactions are not resonant, and therefore can be safely neglected in the ultracold regime. Let us denote the van der Waals range of the interspecies interaction by  $R_e$  and write down the partial wave expansion of the on-shell scattering amplitude [13]

$$f(\mathbf{k}, \mathbf{k}') = \sum_{\ell=0}^{\infty} (2\ell + 1) P_\ell(\cos \theta) f_\ell(k). \quad (1)$$

Here  $\mathbf{k}$  and  $\mathbf{k}'$  are initial and final relative momenta such that  $|\mathbf{k}| = |\mathbf{k}'| = k$ , and  $\theta = \angle_{\mathbf{k}, \mathbf{k}'}$  is the scattering angle. We set  $\hbar = 1$ . The partial wave amplitudes  $f_\ell(k)$  can be written in terms of the phase shifts  $\delta_\ell(k)$  as

$$f_\ell(k) = \frac{1}{k \cot \delta_\ell(k) - ik}. \quad (2)$$

Expanding the denominator of Eq. (2) in powers of  $kR_e$  gives the effective range expansion. In particular, in the  $s$ -wave channel ( $\ell = 0$ ) we have

$$k \cot \delta_0(k) \approx -a^{-1} + \frac{1}{2} r_0 k^2 + \dots, \quad (3)$$

and the corresponding expansion in the  $p$ -wave channel ( $\ell = 1$ ) reads

$$k^3 \cot \delta_1(k) \approx -v^{-1} + \frac{1}{2} k_0 k^2 + \dots, \quad (4)$$

where  $v$  is the  $p$ -wave scattering volume, and  $k_0$  is a parameter analogous to the effective range.

The scale of the scattering length  $a$ , the effective range  $r_0$ , and other expansion parameters in the higher order terms in Eq. (3) are set by the length  $R_e$  or its power of suitable dimension, and the same holds for higher partial waves. For  $k \rightarrow 0$  the partial scattering amplitudes are proportional to  $(kR_e)^{2\ell}$ . Thus, in the limit  $kR_e \ll 1$  (ultracold regime) the  $s$ -wave scattering amplitude, which equals  $f_0(0) = -a$ , is the most important interaction parameter in the mixture.

Near a scattering resonance the scattering length can be modified and, in particular, can take anomalously large values (i.e.  $|a| \gg R_e$ ). A magnetic Feshbach resonance occurs when the collision energy of the two atoms is close to the energy of a quasidiscrete molecular state in another hyperfine domain, which is called closed channel. The tuning of the scattering amplitude is achieved by shifting the open and closed channels with respect to each other in an external magnetic field (hyperfine states corresponding to the open and closed channel have different magnetic moments). The width of the resonance is determined by the strength of the coupling between these two channels. The narrower the resonance, the stronger the collision energy dependence of the scattering amplitude, and, therefore, the larger the effective range  $r_0$ . We call a resonance narrow, if  $|r_0| \gg R_e$  [21]. In fact, near such a resonance  $r_0$  is necessarily negative and it is convenient to use another length parameter [22]

$$R^* = -r_0/2 = \frac{1}{2\mu a_{bg}\mu_{rel}\Delta B}, \quad (5)$$

where  $\mu = m_\uparrow m_\downarrow / (m_\uparrow + m_\downarrow)$  is the reduced mass,  $a_{bg}$  is the background scattering length,  $\mu_{rel}$  is the difference in the magnetic moments of the closed and open channels, and  $\Delta B$  is the magnetic width of the Feshbach resonance. All  ${}^6\text{Li}-{}^{40}\text{K}$  interspecies resonances discussed so far are characterized by  $R^* \gtrsim 100\text{nm}$  [4, 7], which is much larger than the van der Waals range  $R_e \approx 2.2\text{nm}$ .

One can imagine an interatomic potential for which the higher order terms in Eq. (3) are also anomalously large. For example, we can introduce one or several additional closed channels with quasistationary states very close to the open-channel threshold resulting in a rather exotic scattering amplitude [24]. However, in this paper we assume a more practical and simple case in which the terms denoted by  $\dots$  in Eq. (3) vanish in the limit  $kR_e \rightarrow 0$ .

We will also assume that scattering with  $\ell > 0$  is not resonant and can be neglected in this limit. Then, substituting Eq. (3) into Eq. (2) we get the well-known formula for the resonant scattering at a quasidiscrete level [13] (written as a function of momentum rather than energy)

$$f(\mathbf{k}) = -\frac{1}{1/a + R^*k^2 + ik}. \quad (6)$$

The ratio  $R^*/a$  measures the detuning from the resonance and we distinguish the regime of small detuning,  $R^*/a \ll 1$ , and the regime of intermediate detuning,  $R^*/a \gg 1$ . The properties of a few-body system in these two limits are qualitatively different [22].

In order to describe the  $\uparrow\downarrow$  mixture near a narrow resonance we use the two-channel Hamiltonian [25]

$$\hat{H} = \sum_{\mathbf{k},\sigma=\uparrow,\downarrow} \frac{k^2}{2m_\sigma} \hat{a}_{\mathbf{k},\sigma}^\dagger \hat{a}_{\mathbf{k},\sigma} + \sum_{\mathbf{p}} \left( \omega_0 + \frac{p^2}{2M} \right) \hat{b}_{\mathbf{p}}^\dagger \hat{b}_{\mathbf{p}} + \sum_{\mathbf{k},\mathbf{p}} \frac{g}{\sqrt{V}} \left( \hat{b}_{\mathbf{p}}^\dagger \hat{a}_{\frac{\mathbf{p}}{2}+\mathbf{k},\uparrow}^\dagger \hat{a}_{\frac{\mathbf{p}}{2}-\mathbf{k},\downarrow} + \hat{b}_{\mathbf{p}} \hat{a}_{\frac{\mathbf{p}}{2}-\mathbf{k},\downarrow}^\dagger \hat{a}_{\frac{\mathbf{p}}{2}+\mathbf{k},\uparrow}^\dagger \right), \quad (7)$$

where  $a_{\uparrow,\downarrow}^\dagger$  and  $a_{\uparrow,\downarrow}$  are creation and annihilation operators of the two fermionic species while  $b^\dagger$  ( $b$ ) creates (annihilates) a closed-channel molecule of mass  $M \equiv m_\uparrow + m_\downarrow$ . The atom-molecule interconversion amplitude  $g$  is taken constant up to the momentum cut-off  $\Lambda \propto 1/R_e$ , and  $\omega_0$  is the bare detuning of the molecule. The quantities  $a$  and  $R^*$  are related to the parameters of the model (7) by [23] (see also Appendix A)

$$a = \frac{\mu g^2}{2\pi} \frac{1}{\frac{g^2\mu\Lambda}{\pi^2} - \omega_0}, \quad R^* = \frac{\pi}{\mu^2 g^2}. \quad (8)$$

The bare propagators of atoms and closed-channel molecules read

$$G_{\uparrow,\downarrow}(\mathbf{p}, p_0) = \frac{1}{p_0 - p^2/2m_{\uparrow,\downarrow} + i0}, \quad D_0(\mathbf{p}, p_0) = \frac{1}{p_0 - p^2/2M - \omega_0 + i0}, \quad (9)$$

where  $+i0$  slightly shifts the poles of  $G$  and  $D_0$  into the lower half of the complex  $p_0$ -plane. A physical dimer consists of a closed-channel molecule dressed by open-channel atoms. The corresponding propagator is given by (see Appendix A)

$$D(\mathbf{p}, p_0) = \frac{2\pi/\mu}{2\mu R^* \left( p_0 - \frac{p^2}{2M} + i0 \right) + \frac{1}{a} - \sqrt{2\mu} \sqrt{-p_0 + \frac{p^2}{2M} - i0}}. \quad (10)$$

The pole of  $D(0, p_0)$  determines the dimer binding energy

$$\epsilon_0 = -(\sqrt{1 + 4R^*/a} - 1)^2 / 8\mu R^{*2}. \quad (11)$$

Equation (11) interpolates between the two limits: for small detuning we have  $\epsilon_0 \simeq -1/2\mu a^2$  and in the regime of intermediate detuning  $\epsilon_0 \simeq -1/2\mu R^* a$ .

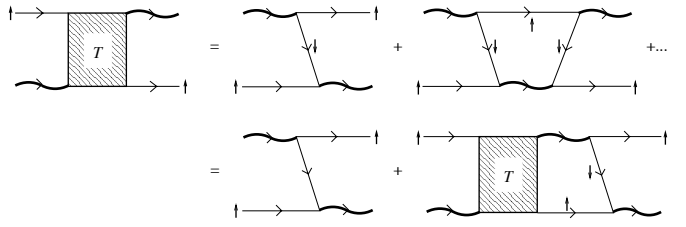


**Fig. 1.** Diagrammatic series contributing to the atom-dimer  $T$ -matrix and a schematic representation of the Skorniakov-Ter-Martirosian integral equation (12). External propagators are included to guide the eye, they do not form part of the  $T$ -matrix. Straight and wavy lines denote atomic and dimer propagators, respectively.

### 3 Atom-dimer scattering

Knowledge of atom-dimer interaction parameters is necessary for the correct description of an atom-molecule mixture on the BEC side of the Feshbach resonance. The momentum-space formalism for the three-body problem with short-range interactions was first demonstrated in the calculation of the neutron-deuteron scattering length (total spin  $S = 3/2$  in this case corresponds to our  $\uparrow\downarrow$  scattering problem) [26]. The coordinate formulation can be found in Ref. [18] where the atom-dimer scattering length was obtained in the mass-imbalanced case. Here we extend these results to higher partial waves, finite collision energies, and finite Feshbach resonance width.

Let us denote the atom-dimer scattering  $T$ -matrix by  $T(\mathbf{k}, k_0; \mathbf{p}, p_0)$ , the arguments of which imply that the incoming four-momenta of the atom and the molecule are  $(\mathbf{k}, k_0)$  and  $(-\mathbf{k}, E - k_0)$ , and the outgoing ones are  $(\mathbf{p}, p_0)$  and  $(-\mathbf{p}, E - p_0)$ , respectively. In Fig. 1 we show the diagrammatic series for  $T$ , the summation of which results in the Skorniakov-Ter-Martirosian integral equation [26] (see also Ref. [27])

$$T(\mathbf{k}, k_0; \mathbf{p}, p_0) = -g^2 Z G_\downarrow(-\mathbf{k} - \mathbf{p}, E - k_0 - p_0) - i \int \frac{d^4 q}{(2\pi)^4} G_\uparrow(\mathbf{q}, q_0) G_\downarrow(-\mathbf{p} - \mathbf{q}, E - p_0 - q_0) \times D(-\mathbf{q}, E - q_0) T(\mathbf{k}, k_0; \mathbf{q}, q_0). \quad (12)$$

Equation (12) is formally identical to the equal-mass wide-resonance one, the difference being hidden in the propagators and the factor  $Z$ , which serves for correct normalization of external propagators (see Appendix A). The atom-dimer elastic scattering amplitude is proportional to the on-shell  $T$ -matrix:

$$f(\mathbf{k}, \mathbf{k}') = -\frac{\mu_3}{2\pi} T(\mathbf{k}, k^2/2m_\uparrow; \mathbf{k}', k'^2/2m_\uparrow), \quad (13)$$

where  $\mu_3 \equiv Mm_\uparrow/(M + m_\uparrow)$  is the reduced mass of the atom-dimer system, and  $k = |\mathbf{k}| = |\mathbf{k}'|$ . Hereafter  $f$ ,  $f_\ell$ ,  $\delta_\ell$ , and  $\sigma_\ell$  refer to the atom-dimer scattering parameters, the two-atom interaction being described by  $a$  and  $R^*$ .

Integration over  $q_0$  in Eq. (12) may be carried out by closing the complex contour in the lower half plane. The integration picks up the contribution from the simple pole

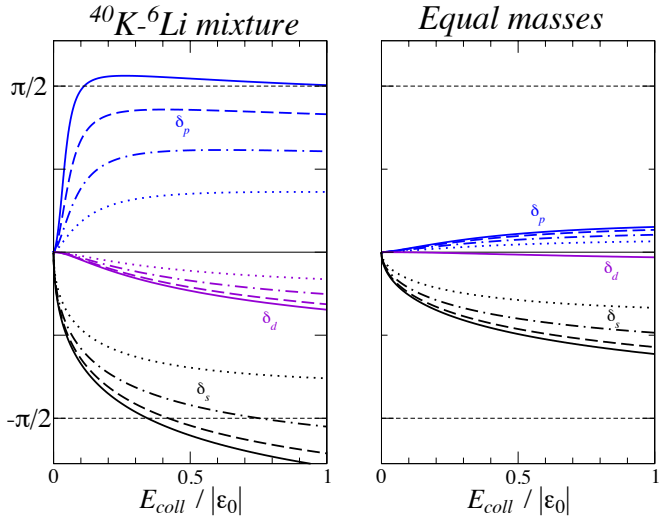


**Fig. 2.** (color online). Atom-dimer  $s$ ,  $p$ , and  $d$ -wave scattering phase shifts vs.  $E_{\text{coll}}/|\epsilon_0|$ . Solid, dashed, dot-dashed, and dotted lines correspond to  $R^*/a = 0, 1/16, 1/4$ , and  $R^* = a$ , respectively. In the homonuclear case we show  $\delta_d$  only for  $R^* = 0$ .

of  $G_\uparrow$  at  $q_0 = q^2/2m_\uparrow$ . The scattering phase shifts are on-shell quantities and we let  $k_0 = k^2/2m_\uparrow$ ,  $p_0 = p^2/2m_\uparrow$ , and the total energy  $E = k^2/2\mu_3 + \epsilon_0$ . The remaining on-shell condition,  $|\mathbf{p}| = |\mathbf{k}|$ , should be implemented at the end of the calculations.

The kernel of the resulting three-dimensional integral equation has a simple pole at  $|\mathbf{q}| = |\mathbf{k}|$  hidden in the dimer propagator. We make it explicit by defining functions  $\tilde{f}$  and  $h$ :

$$\frac{\tilde{f}(\mathbf{k}, \mathbf{q})}{q^2 - k^2 - i0} = \frac{D(\mathbf{q}, E - q^2/2m_\uparrow)}{4\pi g^2 Z} T\left(\mathbf{k}, \frac{k^2}{2m_\uparrow}; \mathbf{q}, \frac{q^2}{2m_\uparrow}\right),$$

$$h(k, q) = (k^2 - q^2)D(\mathbf{q}, E - q^2/2m_\uparrow)/4\pi. \quad (14)$$

Both  $\tilde{f}$  and  $h$  are not singular at  $|\mathbf{q}| = |\mathbf{k}|$ , and  $\tilde{f}$  is chosen such that  $\tilde{f}(\mathbf{k}, \mathbf{k}') = f(\mathbf{k}, \mathbf{k}')$ , for  $|\mathbf{k}| = |\mathbf{k}'|$ . Finally, we note that Eq. (12) conserves angular momentum and, therefore, can be written as a set of decoupled equations for each partial wave

$$\tilde{f}_\ell(k, p) = h(k, p) \left\{ g_\ell(k, p) + \frac{2}{\pi} \int_0^\infty q^2 dq \frac{g_\ell(p, q) \tilde{f}_\ell(k, q)}{q^2 - k^2 - i0} \right\}, \quad (15)$$

where we define

$$g_\ell(k, p) = \frac{1}{2} \int_{-1}^1 dx P_\ell(x) G_\downarrow(\mathbf{k} + \mathbf{p}, E - k^2/2m_\uparrow - p^2/2m_\uparrow), \quad (16)$$

where  $x$  is the cosine of the angle between  $\mathbf{k}$  and  $\mathbf{p}$ . Partial atom-dimer scattering amplitudes are related to solutions of Eq. (15) by the equation  $f_\ell(k) = \tilde{f}_\ell(k, k)$ , and the corresponding phase shifts  $\delta_\ell$  are deduced from Eq. (2).

In Fig. 2 we plot the  $s$ -,  $p$ -, and  $d$ -wave phase shifts as functions of the collision energy  $E_{\text{coll}} = k^2/2\mu_3$  for different detunings  $R^*/a$ . We write the phase shifts as  $\delta_0 \equiv \delta_s$ ,

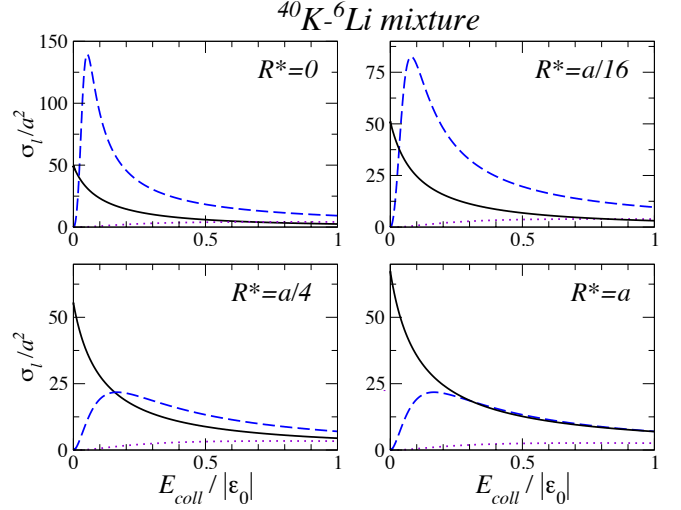


**Fig. 3.** (color online). Partial K-KLi atom-dimer cross-sections  $\sigma_s$  (solid),  $\sigma_p$  (dashed), and  $\sigma_d$  (dotted) in units of  $a^2$  vs. collision energy for different detunings  $R^*/a$ .

$\delta_1 \equiv \delta_p$ , and  $\delta_2 \equiv \delta_d$ . The results are shown for two mass ratios:  $m_\uparrow/m_\downarrow = 6.64$  (left) and  $m_\uparrow/m_\downarrow = 1$  (right). We keep the same vertical scale in both graphs, and one can see that the atom-dimer interaction in the heteronuclear case is stronger in every considered channel. Looking at the low-energy asymptotes of the phase shifts in the wide resonance case ( $R^* = 0$ ) we see that passing from  $m_\uparrow/m_\downarrow = 1$  to  $m_\uparrow/m_\downarrow = 6.64$  the atom-dimer  $s$ -wave scattering length increases from  $a_{\text{ad}} \approx 1.18a$  to  $a_{\text{ad}} \approx 1.98a$ , consistent with Refs. [26] and [18]. At the same time the  $p$ -wave scattering volume increases by more than an order of magnitude from  $v_{\text{ad}} \approx -0.95a^3$  to  $v_{\text{ad}} \approx -10.1a^3$ , which is apparently due to the vicinity of the resonance at the critical mass ratio  $m_\uparrow/m_\downarrow \approx 8.2$  [19]. Although the mass ratio for the K-Li case is quite a bit smaller, our results indicate that for sufficiently small detuning one has a strongly marked  $p$ -wave K-KLi scattering resonance. Indeed, for  $R^* = 0$  the  $p$ -wave phase shift reaches the unitarity value  $\pi/2$  at a relatively small collision energy  $E_{\text{coll}} \approx 0.1|\epsilon_0|$ .

In Fig. 2 we also see that the atom-dimer interaction decreases with detuning. We attribute this to the fact that at larger  $R^*/a$  the light atom spends more time in the closed-channel molecular state, and consequently contributes less to the atom-dimer exchange interaction. In a sense, increasing  $R^*/a$  is similar to increasing the mass of the light atom (decreasing the mass ratio): the heavier the atom, the weaker the exchange interaction.

Although the  $p$ -wave resonance becomes less pronounced near a narrow resonance, in a K-Li mixture the  $p$ -wave atom-dimer interaction can be strong, which is demonstrated in Fig. 3, where we plot the partial wave cross-sections  $\sigma_\ell(k) = 4\pi(2\ell+1)k^{-2} \sin^2 \delta_\ell(k)$ . We clearly see that for detunings  $R^*/a \lesssim 1$  the  $p$ -wave partial cross-section either exceeds or is comparable to  $\sigma_s$  in a wide range of collision energies.

For comparison, in Fig. 4 we present partial atom-dimer cross-sections in the homonuclear case. We see that

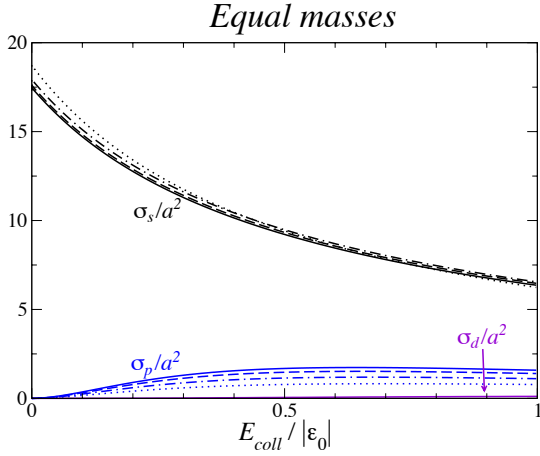


**Fig. 4.** (color online). Atom-dimer *s*-wave (black), *p*-wave (blue), and *d*-wave (purple) scattering cross sections for the homonuclear gas. Solid, dashed, dot-dashed, and dotted lines correspond to  $R^*/a = 0, 1/16, 1/4$ , and  $R^* = a$ , respectively.

the *s*-wave contribution is always dominant and the functional form of  $\sigma_s/a^2$  is fairly insensitive to the detuning.

We have calculated the scattering parameters for several higher partial waves. Their contributions rapidly decrease with  $\ell$  and it is worth plotting only the *d*-wave phase shifts (see Fig. 2) and scattering cross-sections (Figs. 3 and 4). The *d*-wave contribution is comparable to the *s*- and *p*-wave ones only in the heteronuclear case and for relatively high collision energies  $\sim |\epsilon_0|$ . In Figs. 2 and 4 the *d*-wave contribution for the homonuclear case is plotted only for  $R^* = 0$  as for finite detunings the curves are even closer to the horizontal axis.

We have already discussed the atom-dimer scattering length and scattering volume for  $m_\uparrow/m_\downarrow \approx 6.64$  and  $m_\uparrow/m_\downarrow = 1$  in the case  $R^* = 0$ . In Figs. 5 and 6 we plot these quantities and the effective range parameters  $r_{\text{ad}}$  and  $k_{\text{ad}}$  [atom-dimer analogues of  $r_0$  and  $k_0$  defined in Eqs. (3) and (4)] versus the detuning  $R^*/a$ . Dotted lines in these graphs are obtained by using a perturbation theory in the limit of a very narrow resonance,  $g \rightarrow 0$ , when the atom-dimer *T*-matrix can be obtained by summing the first few diagrams in Fig. 1. This gives an expansion in powers of  $\sqrt{a/R^*} \ll 1$ . The first two terms in the expansion of  $a_{\text{ad}}$  and  $v_{\text{ad}}$  and the leading terms for the effective range parameters  $r_{\text{ad}}$  and  $k_{\text{ad}}$  read

$$a_{\text{ad}} \approx a \frac{\mu_3}{\mu} \left[ 1 + \frac{1}{2} \left( 1 - \frac{\mu_3}{\mu} \right) \sqrt{\frac{a}{R^*}} \right], \quad (17)$$

$$r_{\text{ad}} \approx -4R^* \frac{\mu}{\mu_3} \left( 1 - \frac{\mu}{2\mu_3} \right), \quad (18)$$

$$v_{\text{ad}} \approx -\frac{2}{3} a^2 R^* \frac{\mu_3}{m_\downarrow} \left[ 1 + \frac{3}{2} \left( 1 + \frac{\mu_3}{36m_\downarrow} \right) \sqrt{\frac{a}{R^*}} \right], \quad (19)$$

$$k_{\text{ad}} \approx \frac{12 m_\downarrow}{a} \frac{\mu}{\mu_3} \left( 1 - \frac{\mu}{2\mu_3} \right). \quad (20)$$

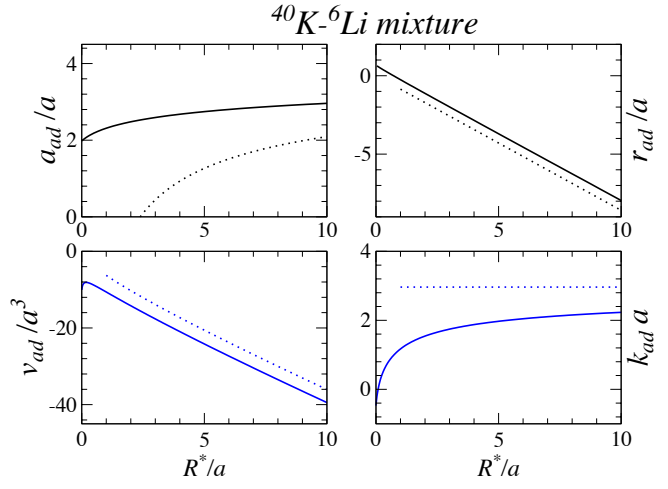


**Fig. 5.** (color online). Atom-dimer scattering length  $a_{\text{ad}}$ , *s*-wave effective range  $r_{\text{ad}}$ , *p*-wave scattering volume  $v_{\text{ad}}$ , and the *p*-wave effective range parameter  $k_{\text{ad}}$  in units of corresponding powers of  $a$  vs.  $R^*/a$  for  $m_\uparrow/m_\downarrow = 6.64$ . Solid lines are exact and dotted lines are approximate results (17)-(20) valid in the limit  $R^* \gg a$ .

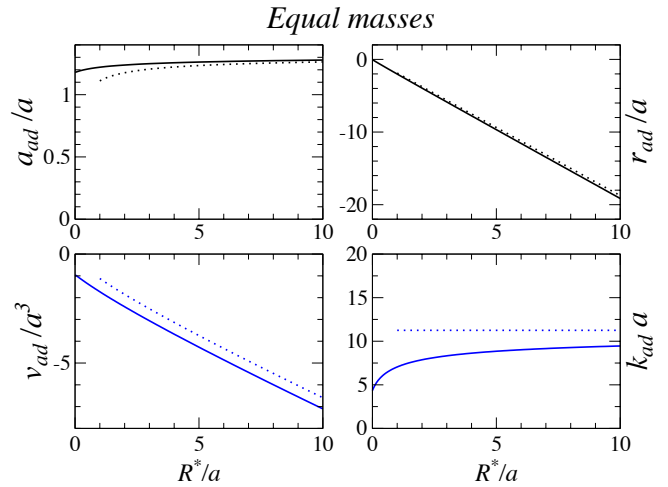


**Fig. 6.** (color online). Same as in Fig. 5 but for the homonuclear case.

### 3.1 Born-Oppenheimer approximation

It is instructive to consider the enhancement of the atom-dimer scattering and the appearance of trimers for sufficiently large mass ratios in the Born-Oppenheimer approximation [28]. This method was introduced in Ref. [15] to study Efimov physics in the system of one light and two heavy particles. Although the Born-Oppenheimer approximation is not exact, it serves well to illustrate the essential physics leading to the resonant enhancement of the *p*-wave scattering. Here we extend it to the case of a resonance.

The method takes advantage of the large mass ratio by assuming that the state of the light atom adiabatically adjusts itself to the distance  $\mathbf{R}$  between the heavy fermions. The wavefunction of the light atom can be written in the

form

$$\psi_{\mathbf{R},\pm}(\mathbf{r}) \propto \frac{e^{-\kappa_{\pm}(R)|\mathbf{r}-\mathbf{R}/2|/R}}{|\mathbf{r}-\mathbf{R}/2|} \pm \frac{e^{-\kappa_{\pm}(R)|\mathbf{r}+\mathbf{R}/2|/R}}{|\mathbf{r}+\mathbf{R}/2|}. \quad (21)$$

It satisfies the free-particle Schrödinger equation with the energy

$$\epsilon_{\pm}(R) = -\kappa_{\pm}^2(R)/2m_{\downarrow}. \quad (22)$$

The singularities of  $\psi_{\mathbf{R},\pm}(\mathbf{r})$  at vanishing  $\tilde{\mathbf{r}} = \mathbf{r} \pm \mathbf{R}/2$  satisfy the Bethe-Peierls boundary condition [29]

$$[\tilde{r}\psi]'/\tilde{r}\psi \Big|_{\tilde{r} \rightarrow 0} = i\kappa_{\pm}(R) \cot \delta_0 [i\kappa_{\pm}(R)] \\ = -1/a + R^* \kappa_{\pm}^2(R), \quad (23)$$

where the light-heavy  $s$ -wave phase shift, again denoted by  $\delta_0$ , is calculated at the light-heavy collision energy  $\epsilon_{\pm}(R)$ . The equation for  $\kappa_{\pm}(R)$  is obtained by applying the boundary condition (23) to the wavefunction (21):

$$\kappa_{\pm}(R) \mp \exp[-\kappa_{\pm}(R)R]/R = 1/a - R^* \kappa_{\pm}^2(R). \quad (24)$$

The second step of the Born-Oppenheimer method consists of solving the Schrödinger equation for the heavy fermions by using  $\epsilon_{\pm}(R)$  as the potential energy surface. Let us denote the corresponding heavy-fermion wavefunction by  $\phi(\mathbf{R})$ . Since the total three-body wavefunction, proportional to the product  $\phi(\mathbf{R})\psi_{\mathbf{R},\pm}(\mathbf{r})$ , should be antisymmetric with respect to the permutation of the heavy fermions, the symmetry of  $\phi$  depends on the choice of sign in Eq. (21). As  $\psi_{\mathbf{R},+}(\mathbf{r})$  is symmetric with respect to the permutation  $\mathbf{R} \leftrightarrow -\mathbf{R}$ , the heavy-atom wavefunction  $\phi$  is antisymmetric and describes odd atom-dimer scattering channels. Accordingly, the lower sign in Eqs. (21-24) corresponds to even channels. We see how the composite nature of the dimer leads to the  $\ell$ -dependent effective atom-dimer potentials: by solving Eq. (24) one arrives at a purely attractive  $\epsilon_+(R)$  for odd channels and purely repulsive  $\epsilon_-(R)$  for even ones.

From the viewpoint of the radial Schrödinger equation it is convenient to introduce the total effective potential for each  $\phi_{\ell}(R)$ :

$$V_{\ell}(R) = \epsilon_{(-1)^{\ell+1}}(R) - \epsilon(\infty) + \ell(\ell+1)/m_{\uparrow}R^2, \quad (25)$$

which includes the centrifugal barrier and shifts the threshold to zero by subtracting the dimer binding energy

$$\epsilon(\infty) = -(\sqrt{1+4R^*/a} - 1)^2/8m_{\downarrow}R^{*2}. \quad (26)$$

In the limit  $m_{\uparrow} \gg m_{\downarrow}$  Eq. (26) reduces to Eq. (11).

For the  $p$ -wave atom-dimer interaction the central issue is the competition between the attractive exchange potential  $\epsilon_+ \propto 1/m_{\downarrow}$  and the repulsive centrifugal barrier, which is inversely proportional to  $m_{\uparrow}$ . In Fig. 7 we show  $V_1(R)$  in the limit of vanishing detuning for different mass ratios. Remarkably, for  $m_{\uparrow}/m_{\downarrow} \sim m_K/m_{Li}$  this potential, being repulsive in both limits  $R \ll a$  and  $R \gg a$ , develops a well at distances  $R \sim a$ . For  $m_{\uparrow}/m_{\downarrow} > 8.2$  the depth of this well is enough to accommodate a trimer state with unit angular momentum [19] and for somewhat smaller

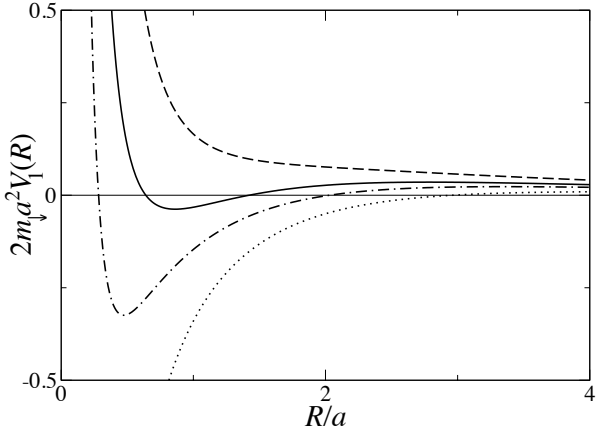


**Fig. 7.** The Born-Oppenheimer atom-dimer effective potential  $V_1(R)$  [in units of  $1/2m_{\downarrow}a^2$ ] in the wide resonance case ( $R^* = 0$ ) for mass ratios  $m_{\uparrow}/m_{\downarrow} = 5$  (dashed),  $m_K/m_{Li}$  (solid), 8.2 (dash-dotted), and 13.6 (dotted).

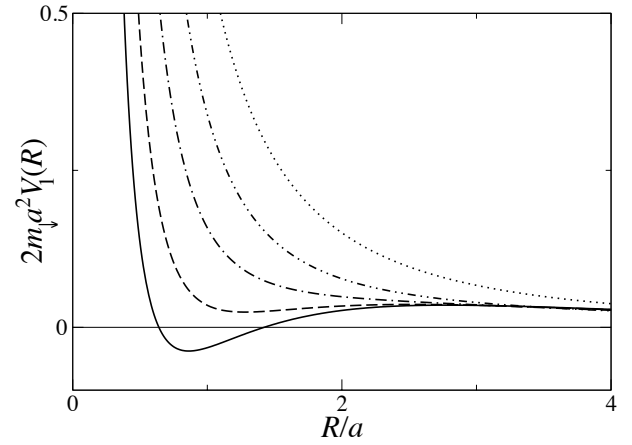


**Fig. 8.** The Born-Oppenheimer atom-dimer effective potential  $V_1(R)$  [in units of  $1/2m_{\downarrow}a^2$ ] in the K-Li case for  $R^* = 0$  (solid),  $R^* = a/16$  (dashed),  $R^* = a/4$  (dash-dotted), and  $R^* = a$  (double-dot dashed). The dotted line is the centrifugal barrier.

mass ratios the presence of the well leads to the resonant enhancement of the  $p$ -wave interaction.

The effect of finite  $R^*$  is to decrease the strength of the exchange potentials  $\epsilon_{\pm}$ . In Fig. 8 we show  $V_1(R)$  in the K-Li case for different values of the detuning  $R^*/a$ . One can see that the  $p$ -wave attraction becomes less pronounced and the well eventually disappears with increasing  $R^*/a$ .

It is important to distinguish the  $p$ -wave trimer for  $m_{\uparrow}/m_{\downarrow} \gtrsim 8.2$  from Efimov trimers. The former exists only for  $a > 0$  and is a result of the peculiar competition between the exchange potential and the centrifugal force at distances of the order of  $a$ , which determines its size. In contrast, the Efimov effect occurs at larger mass ratios,  $m_{\uparrow}/m_{\downarrow} > 13.6$ , when the effective potential at distances  $R \ll a$  is no longer repulsive. Then, in the Born-Oppenheimer description the heavy atoms fall to the center in an attractive  $1/R^2$ -potential. This is accompanied

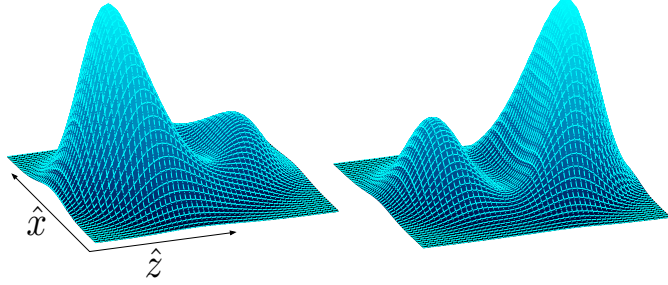


**Fig. 9.** (color online). The integrated column density for K-KLi atom-dimer scattering in arbitrary units. The collision energies are  $E_{\text{coll}} = 0.05|\epsilon_0|$  (left) and  $E_{\text{coll}} = 0.25|\epsilon_0|$  (right). In both cases  $R^* = a/4$ . Backward direction corresponds to negative  $z$ . For presentation purposes we imitate a small thermal smear.

by the appearance of an infinite set of Efimov states, irrespective of the sign of  $a$ .

Atom-dimer scattering in even channels is described by the potential  $\epsilon_+(R)$ , which is defined at distances  $R > a$ . It has a form of a purely repulsive soft-core potential, which increases with the mass ratio and decreases with  $R^*$ , consistent with the exact results above on  $s$ - and  $d$ -wave atom-dimer scattering.

### 3.2 Interference of $s$ - and $p$ -waves

Now we would like to discuss one of the implications of the channel dependent atom-dimer interaction, a peculiarity, which is strongly pronounced in the K-Li mixture. In this case the  $p$ - and  $s$ -wave phase shifts are comparable in magnitude and can be large (see Fig. 3). It is thus not necessary to go to very high collision energies for observing the quantum interference between these partial waves [30].

Let us consider a *gedankenexperiment* in which a cold thermal cloud of KLi dimers collides with a cloud of K atoms at collision energies below the dimer break-up threshold. The measurable quantity is then the angular distribution of scattered dimers (or atoms), which is proportional to the differential cross-section. We can write it in terms of the phase shifts by using Eqs. (1) and (2):

$$\frac{d\sigma}{d\Omega} = \frac{1}{k^2} [\sin^2 \delta_s + 6 \cos(\delta_p - \delta_s) \sin \delta_s \sin \delta_p \cos \theta + 9 \sin^2 \delta_p \cos^2 \theta] + \dots \quad (27)$$

Here  $k$  is the relative atom-dimer momentum and the angle  $\theta$  is measured with respect to the collision axis, which we denote by  $\hat{z}$ . The dots signify the contribution of higher partial waves. We have checked that they can be safely ignored.

The first term on the right hand side in Eq. (27) gives the well-known spherically symmetric scattering halo. The last term corresponds to the pure  $p$ -wave scattering. It contributes equally to the forward ( $0 < \theta < \pi/2$ ) and backward ( $\pi/2 < \theta < \pi$ ) directions, but vanishes in the direction perpendicular to  $\hat{z}$ . The second (interference) term

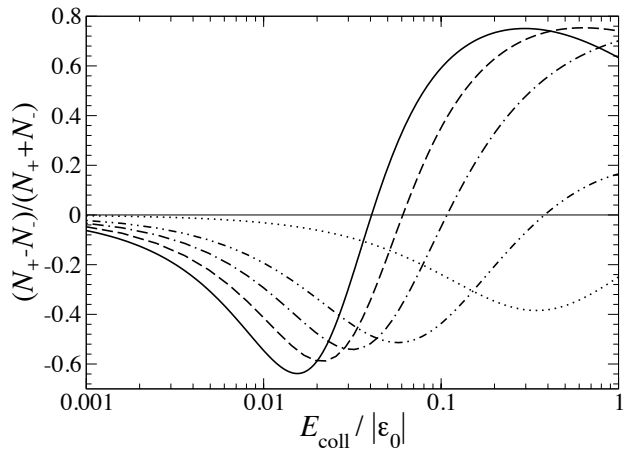


**Fig. 10.** The contrast vs. collision energy for detuning  $R^*/a$  equal to 0 (solid),  $1/16$  (dashed),  $1/4$  (dot-dashed), and  $1$  (double-dot dashed). Dotted line is the homonuclear case result for  $R^* = 0$ .

favors either backward or forward scattering. In Fig. 9 we simulate an absorption image (column density) of scattered particles that initially moved in the positive  $z$  direction. In the K-Li case backward scattering dominates at small collision energies while forward scattering is favored at higher energies, when  $\delta_p - \delta_s > \pi/2$ .

In Fig. 10 we plot the contrast, defined as the normalized difference between the numbers of particles scattered forward,  $N_+$ , and backward,  $N_-$ , as a function of collision energy for different detunings  $R^*/a$ . For comparison we also present the homonuclear wide-resonance case (dotted line). We see that in this case backward scattering always dominates, the highest contrast achieved for  $E_{\text{coll}} \approx |\epsilon_0|/3$ .

The collision experiment described above requires the ability of manipulating atoms and molecules individually, which points to an advantage of heteronuclear mixtures – in the heteronuclear case different atomic species feel optical potentials in a different manner, and this obviously holds for the two components of the corresponding atom-molecule mixture.

As far as the energy scale is concerned, in the K-Li case with  $R^* = a = 100$  nm the dimer binding energy given by Eq. (11) equals  $|\epsilon_0| \approx 1.8 \mu\text{K}$ , and it decreases to 200 nK when  $a = 400$  nm. We also mention, for reference, that the relative atom-dimer velocities corresponding to the collision energy  $E_{\text{coll}} = |\epsilon_0|$  in these two cases equal 3.7 cm/s and 1.2 cm/s respectively.

## 4 Dimer-dimer scattering

Dimer-dimer interaction parameters are crucial for the description of the BCS-BEC crossover in the BEC-limit, i.e. when the gas of molecules is dilute. In the lowest order the chemical potential, condensate depletion, and speed of sound in the BEC of dimers are determined from the density and dimer-dimer scattering length  $a_{dd}$  in the same manner [31] as in the usual Bogoliubov theory of dilute Bose gases.

In the case of a homonuclear mixture near a wide resonance the dimer-dimer scattering length equals  $a_{dd} \approx 0.6a$ . This number was obtained in Ref. [32] by solving an integral equation derived directly from the four-body Schrödinger equation in coordinate space. Later the result was confirmed by diagrammatic approaches [31, 33] and by Monte-Carlo and variational techniques [34, 35]. In the heteronuclear case the molecule-molecule scattering length was also calculated in the case of a wide interspecies resonance [36, 35, 37]. Von Stecher *et al.* [35] also computed the dimer-dimer effective range. The inelastic scattering and the formation of Efimov trimers in dimer-dimer collisions for  $m_\uparrow/m_\downarrow > 13.6$  is discussed in Ref. [38].

A qualitative summary of the results cited above is that the dimer-dimer interaction can be thought of as a soft-core repulsion. It strengthens with the mass ratio, but is always weaker than the  $s$ -wave repulsion between a dimer and a heavy atom. This picture can be understood from the Born-Oppenheimer analysis, when one assumes that the wavefunction of the two light fermions is given by the antisymmetrized product of  $\psi_{R,+}(\mathbf{r}_1)$  and  $\psi_{R,-}(\mathbf{r}_2)$  [see Eq. (21)], which is antisymmetric under the permutation of the heavy fermions. Accordingly, the heavy-atom part of the wavefunction should be symmetric, consistent with the fact that only even scattering channels are allowed between identical bosons. The Born-Oppenheimer potential energy surface is given, independent of the angular momentum, by the sum  $\epsilon_+(R) + \epsilon_-(R)$ . It increases with decreasing the mass of the light atom and is repulsive, but not as strong as the atom-dimer  $s$ -wave potential  $\epsilon_-(R)$ .

As far as we know, higher partial waves in scattering of bosonic dimers have not been studied, but it has been shown that the ground state of four  $\uparrow - \uparrow - \downarrow - \downarrow$  fermions in an anisotropic harmonic potential has zero angular momentum, independent of  $a$  and the mass ratio [35, 39]. Besides, the qualitative Born-Oppenheimer analysis does not provide arguments for any resonant enhancement of higher partial waves. We thus conjecture that the  $s$ -wave channel should dominate the dimer-dimer interaction, at least for sufficiently small collision energies.

The aim of this section is to compute the dimer-dimer  $s$ -wave scattering length  $a_{dd}$  for the homonuclear and heteronuclear cases (having in mind the Li-K mixture) taking into account the finite width of the Feshbach resonance. Our derivation follows Refs. [31, 37] where the problem was studied in the regime of small detuning.

We consider the scattering of two dimers with four-momenta  $(\mathbf{0}, \epsilon_0)$  into dimers with  $(\pm \mathbf{p}, \epsilon_0 \pm p_0)$  and project onto the  $s$ -wave (average over directions of  $\mathbf{p}$ ). The four-body  $T$ -matrix with these kinematics is denoted  $T(p, p_0)$ . Similarly to the three-body case the four-body  $T$ -matrix consists of an infinite sum of diagrams, which may again be reduced to integral equations. In order to perform this summation, we first construct the sum of two-dimer irreducible diagrams beginning and ending in two dimer propagators. These are the diagrams that cannot be divided in two by cutting only one pair of dimer propagators (external lines are excluded from the summation).

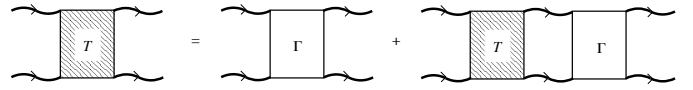


**Fig. 11.** Diagrammatic representation of the integral equation (28), which relates the dimer-dimer  $T$ -matrix with the sum of all the two-dimer irreducible diagrams,  $\Gamma$ .

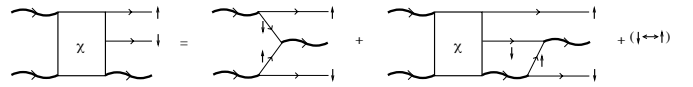


**Fig. 12.** The integral equation satisfied by  $\chi$ , the sum of the two-dimer irreducible diagrams, in which one of the outgoing dimers is split into its constituent parts.

The corresponding  $s$ -wave averaged sum is denoted by  $\Gamma(q, q_0; p, p_0)$ , where the four-momenta of the incoming [outgoing] dimers equal  $(\pm \mathbf{q}, \epsilon_0 \pm q_0)$  [ $(\pm \mathbf{p}, \epsilon_0 \pm p_0)$ ]. The equation for the  $T$ -matrix then reads

$$T(p, p_0) = g^4 Z^2 \Gamma(0, 0; p, p_0) + \frac{i}{4\pi^3} \int q^2 dq dq_0 T(q, q_0) \times \Gamma(q, q_0; p, p_0) D(q, \epsilon_0 + q_0) D(q, \epsilon_0 - q_0) \quad (28)$$

and is illustrated in Fig. 11. As in the three-body case, the prefactor of the first term on the right hand side serves for the correct normalization of external propagators. In order to avoid poles and branch cuts we solve Eq. (28) by rotating the contour of the  $q_0$ -integration to the imaginary axis [31].

The sum of the two-dimer irreducible diagrams is calculated as follows. We first sum the two-dimer irreducible diagrams which end in a dimer and two fermionic atoms. We denote the sum of such two-dimer irreducible diagrams by  $\chi(q, q_0; \mathbf{p}_1, \mathbf{p}_2)$ , where the two incoming dimers have four-momenta  $(\pm \mathbf{q}, \epsilon_0 \pm q_0)$ , and the outgoing  $\uparrow$  [↓] atom may be put on-shell with four-momentum  $(\mathbf{p}_1, p_1^2/2m_\uparrow)$  [ $(\mathbf{p}_2, p_2^2/2m_\downarrow)$ ]. By energy-momentum conservation the outgoing dimer then has four-momentum  $(-\mathbf{p}_1 - \mathbf{p}_2, 2\epsilon_0 - p_1^2/2m_\uparrow - p_2^2/2m_\downarrow)$ . In Fig. 12 we illustrate the integral equation satisfied by  $\chi$ . The equation itself reads

$$\begin{aligned} \chi(q, q_0; \mathbf{p}_1, \mathbf{p}_2) = & - \int \frac{d\Omega_q}{4\pi} \left\{ G_\downarrow \left( \mathbf{q} - \mathbf{p}_1, \epsilon_0 + q_0 - \frac{p_1^2}{2m_\uparrow} \right) \right. \\ & \times G_\uparrow \left( -\mathbf{q} - \mathbf{p}_2, \epsilon_0 - q_0 - \frac{p_2^2}{2m_\downarrow} \right) + [(\mathbf{q}, q_0) \leftrightarrow -(\mathbf{q}, q_0)] \left. \right\} \\ & - \int \frac{d^3 Q}{(2\pi)^3} \left\{ G_\uparrow \left( \mathbf{Q} + \mathbf{p}_1 + \mathbf{p}_2, 2\epsilon_0 - \frac{Q^2}{2m_\downarrow} - \frac{p_1^2}{2m_\uparrow} - \frac{p_2^2}{2m_\downarrow} \right) \right. \\ & \times D \left( \mathbf{Q} + \mathbf{p}_1, 2\epsilon_0 - \frac{Q^2}{2m_\downarrow} - \frac{p_1^2}{2m_\uparrow} \right) \chi(q, q_0; \mathbf{p}_1, \mathbf{Q}) \\ & + G_\downarrow \left( \mathbf{Q} + \mathbf{p}_1 + \mathbf{p}_2, 2\epsilon_0 - \frac{Q^2}{2m_\uparrow} - \frac{p_1^2}{2m_\uparrow} - \frac{p_2^2}{2m_\downarrow} \right) \\ & \left. \times D \left( \mathbf{Q} + \mathbf{p}_2, 2\epsilon_0 - \frac{Q^2}{2m_\uparrow} - \frac{p_2^2}{2m_\downarrow} \right) \chi(q, q_0; \mathbf{Q}, \mathbf{p}_2) \right\}, \end{aligned} \quad (29)$$

where the frequency integration in the closed loop of the iterated term is already performed. The configurational

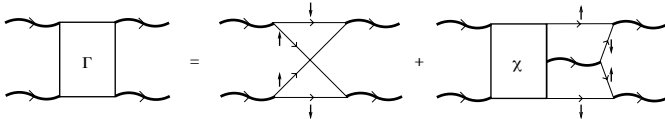


**Fig. 13.**  $\Gamma$  expressed in terms of  $\chi$  (see text).

space of Eq. (29) is in fact three-dimensional. It consists of the moduli of the vectors  $\mathbf{p}_1$  and  $\mathbf{p}_2$ , and the angle between them. The pair  $(q, q_0)$  enters parametrically. In order to express  $\Gamma$  in terms of  $\chi$ , it is advantageous to separate out the simplest diagram, in which the dimers exchange identical atoms. Then, the remaining diagrams in  $\Gamma$  are obtained by closing the fermionic loop in  $\chi$  (see Fig. 13).

The relation between  $\Gamma$  and  $\chi$  is

$$\begin{aligned} \Gamma(q, q_0; p, p_0) &= \Gamma^{(0)}(q, q_0; p, p_0) \\ &- \frac{1}{2} \int \frac{d^3 p_1}{(2\pi)^3} \frac{d^3 p_2}{(2\pi)^3} \left\{ G_{\downarrow} \left( \mathbf{p} - \mathbf{p}_1, \epsilon_0 + p_0 - \frac{p_1^2}{2m_{\uparrow}} \right) \right. \\ &\times G_{\uparrow} \left( \mathbf{p} + \mathbf{p}_2, \epsilon_0 - p_0 - \frac{p_2^2}{2m_{\downarrow}} \right) + [(\mathbf{p}, p_0) \leftrightarrow -(\mathbf{p}, p_0)] \left. \right\} \\ &\times D \left( \mathbf{p}_1 + \mathbf{p}_2, 2\epsilon_0 - \frac{p_1^2}{2m_{\uparrow}} - \frac{p_2^2}{2m_{\downarrow}} \right) \chi(q, q_0; \mathbf{p}_1, \mathbf{p}_2), \quad (30) \end{aligned}$$

where the factor  $\frac{1}{2}$  is needed for correct counting of diagrams. The quantity  $\Gamma^{(0)}$  is the first diagram on the right hand side of Fig. 13 and is given in Appendix B.

The dimer-dimer scattering length is related to the  $T$ -matrix by

$$a_{dd} = \frac{M}{4\pi} T(0, 0). \quad (31)$$

Fig. 14 shows our results for the dimer-dimer scattering length in the equal mass case and for the Li-K mixture. In the limit of small detuning we recover the results [32, 36, 35, 37]

$$a_{dd} = 0.60, \quad m_{\uparrow}/m_{\downarrow} = 1, \quad (32)$$

$$a_{dd} = 0.89, \quad m_{\uparrow}/m_{\downarrow} = m_K/m_{Li}. \quad (33)$$

In the opposite limit the diagrammatic expansion becomes perturbative as is the case for the atom-dimer problem discussed in Sec. 3. The dominant contribution to the dimer-dimer  $T$ -matrix is provided by  $\Gamma^{(0)}$ . Including also the next order, we find [40]

$$\frac{a_{dd}}{a} = \frac{M}{8\mu} \sqrt{\frac{a}{R^*}} + \frac{a}{R^*} \times \begin{cases} 0.13, & m_{\uparrow} = m_{\downarrow} \\ 0.23, & m_{\uparrow}/m_{\downarrow} = 6.64 \end{cases}, \quad R^* \gg a. \quad (34)$$

The first term on the right hand side of Eq. (34) has been derived in the equal-mass case in Ref. [23].

## 5 Relaxation rates

The weakly bound dimers that we are considering are in fact molecules in the highest rovibrational state. They can

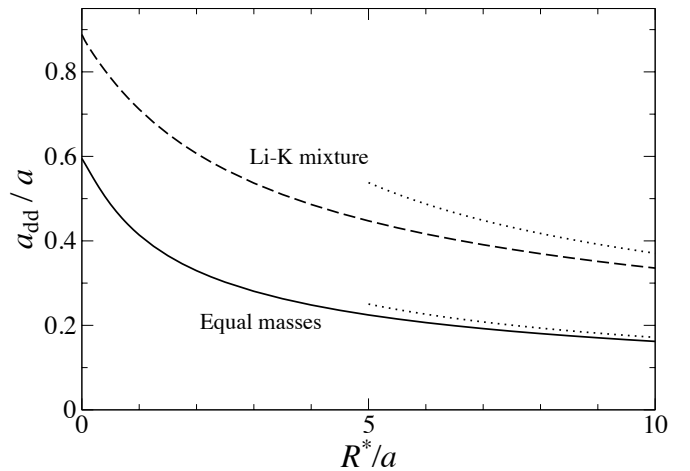


**Fig. 14.** The dimer-dimer scattering length vs.  $R^*/a$  for equal masses (solid line) and for the Li-K mixture (dashed). The dotted lines correspond to the asymptote (34) valid in the limit  $R^* \gg a$ .

undergo relaxation into deep bound states in collisions with each other or with unbound atoms. The process is local as it requires at least three atoms to approach each other to a distance comparable to the size of the future molecular state, i.e.  $\sim R_e$ . The released binding energy is of the order of  $1/m_{\downarrow} R_e^2$  and is much larger than all other energy scales in the problem including the height of the trapping potential. Thus, the relaxation products are lost.

Although the relaxation is a short-range phenomenon, it can be treated in the zero-range approximation. For wide resonances in the Efimov case, i.e. for bosons or for fermions with  $m_{\uparrow}/m_{\downarrow} > 13.6$ , the Efimov physics is well described by the motion of three atoms in an effective attractive  $1/R^2$  potential [41, 42]. The three-body wavefunction can be separated in an incoming wave and an outgoing one, and the relaxation process is taken into account by adding an imaginary part to the three-body parameter [43]. It fixes the ratio of the corresponding incoming and outgoing fluxes. The physical range of the potential  $R_e$  does not enter the resulting relaxation rate constant.

The suppression of relaxation in the non-Efimovian cases (i.e. the  $\uparrow\downarrow\downarrow$  system of fermions with  $m_{\uparrow}/m_{\downarrow} < 13.6$ ) originates from the centrifugal barrier for identical fermions, which, in turn, leads to the repulsive effective three-body  $1/R^2$  potential [14, 44]. In order to recombine, the atoms have to tunnel under this barrier to distances  $\sim R_e$ . The zero-range approach in this case is perturbative. It uses the unperturbed few-body wavefunction to predict the probability of finding three atoms at small distances and gives the functional dependence of the relaxation rate constant on the scattering length for a given mass ratio [17, 36]. If the relaxation rate constant is known for a certain  $a$ , one can predict its value for any other  $a \gg R_e$ .

To be more specific, let us demonstrate how one can estimate the atom-dimer relaxation rate in the case of a wide resonance, for example in  $s$ -wave collisions. For an

atom and a molecule in a unit volume, the probability of finding them within the distance  $a$  from each other equals  $a^3$  (we assume that there is no  $s$ -wave atom-dimer resonance). At distances smaller than  $a$ , the three-body wavefunction (in the center-of-mass reference frame) factorizes into  $\Psi(\mathbf{R}_1, \mathbf{R}_2, \mathbf{r}) \propto \rho^{\nu_s-1} \Phi(\hat{\Omega})$ , where the hyperradius is  $\rho = \sqrt{(\mathbf{R}_1 - \mathbf{R}_2)^2 + m_\downarrow/(2m_\downarrow + m_\uparrow)(2\mathbf{r} - \mathbf{R}_1 - \mathbf{R}_2)^2}$ ,  $\hat{\Omega}$  is a five-dimensional set of all the remaining coordinates (hyperangles), and  $\Phi$  is a normalized hyperangular wavefunction. The power  $\nu_s$  for the  $\downarrow\downarrow\uparrow$ -system is given by the root of the transcendental equation [14]

$$(\nu_s + 1) \tan \frac{\pi \nu_s}{2} - 2 \frac{\sin[\phi(\nu_s + 1)]}{\sin(2\phi) \cos(\pi \nu_s / 2)} = 0 \quad (35)$$

in the interval  $-1 < \text{Re } \nu_s < 3$ . In Eq. (35)  $\phi$  is defined as  $\phi = \arcsin[m_\uparrow/(m_\uparrow + m_\downarrow)]$ . For  $m_\uparrow/m_\downarrow = 1$  we obtain  $\nu_s \approx 1.166$  and for  $m_\uparrow/m_\downarrow = 6.64$  we get  $\nu_s \approx 2.02$ .

The probability of finding the three atoms at hyperradii smaller than  $\rho$  scales with  $\rho$  as  $P(\rho) \propto |\rho^{\nu_s-1}|^2 \rho^6$ . The last term is the volume factor of the six-dimensional configurational space of the three-body problem (in the center-of-mass reference frame). Thus, the total probability of finding the three atoms in the relaxation region is  $\sim a^3 P(R_e)/P(a) \approx a^3 (R_e/a)^{2\nu_s+4}$ . The relaxation rate constant is obtained by multiplying this probability by the frequency with which the relaxation process takes place once the atoms are within the range of the potential. It can be estimated as  $\sim 1/m_\downarrow R_e^2$ . Finally, for the rate constant we obtain

$$\alpha_s^{\text{ad}} \sim \frac{R_e}{m_\downarrow} \left( \frac{R_e}{a} \right)^{2\nu_s+1}. \quad (36)$$

In the case of a narrow resonance the three atoms can approach the recombination region either as free atoms or as a closed-channel molecule and an atom. One can show, however, that in this case the probability of the former is much smaller than the probability of the latter. Indeed, let us consider two atoms,  $\uparrow$  and  $\downarrow$ , in the center-of-mass reference frame. The state of the system is given by

$$|\Psi\rangle = \left( \sum_{\mathbf{k}} \psi_{\mathbf{k}} \hat{a}_{\mathbf{k},\uparrow}^\dagger \hat{a}_{-\mathbf{k},\downarrow}^\dagger + \phi_0 \hat{b}_0^\dagger \right) |0\rangle. \quad (37)$$

Demanding that Eq. (37) be an eigenstate of the Hamiltonian (7) with energy  $E$  we get two coupled equations for  $\psi_{\mathbf{k}}$  and  $\phi_0$ , one of which in coordinate space reads

$$-\frac{\nabla_{\mathbf{R}}^2}{2\mu} \psi(\mathbf{R}) + g\phi_0 \delta(\mathbf{R}) = E\psi(\mathbf{R}). \quad (38)$$

From Eq. (38) one can see that the singularity of  $\psi(\mathbf{R})$  at the origin is related to  $\phi_0$  by

$$\psi(\mathbf{R} \rightarrow 0) = \phi_0 / \sqrt{4\pi R^*} R, \quad (39)$$

where we have used the second of Eqs. (8) to express  $g$  in terms of  $R^*$ .

Using Eq. (39) it is straightforward to show that the wavefunction of the weakly bound molecular state is given by

$$\phi_{0,\text{b}} = \sqrt{Z} = \sqrt{1 - 1/\sqrt{1 + 4R^*/a}} \quad (40)$$

and

$$\psi_{\text{b}}(R) = \sqrt{1 - Z} \sqrt{\kappa/2\pi} \exp(\kappa R)/R, \quad (41)$$

where  $\kappa = \sqrt{2\mu\epsilon_0}$  [see Eq. (11)] and  $Z$  is defined in Eq. (65). We see that the probability of finding the atoms in the open channel equals  $1 - Z$  and is small in the regime of intermediate detuning. Therefore, as  $R^*/a \rightarrow \infty$  the relaxation rate constant tends to a constant value [45]

$$\alpha_{s,\text{bare}}^{\text{ad}} \sim R_e/m_\downarrow, \quad (42)$$

which corresponds to the relaxation in collisions of atoms and bare molecules.

Equation (39) can be used in a more general situation as it applies to a pair of atoms when they are very close to each other. Even in a system of more than two atoms and/or in an external potential we can look at a particular pair of atoms and observe that the probability of finding them in the open channel at separations smaller than  $R$  equals  $\int_0^R |\psi(\mathbf{R}')|^2 4\pi R'^2 dR' = |\phi_0|^2 R/R^*$ , i.e. in the case  $R \ll R^*$  it is much smaller than the probability of finding them in the closed channel. In particular, we can conclude that locally, when three atoms are at the hyperradius  $\rho \ll R^*$ , they can be considered as an atom and a closed-channel molecule. The bare interaction between them is neglected in Eq. (7) as it is assumed non-resonant. Their induced interaction (via the exchange of the open-channel atoms) has a Coulomb form [22, 46] and can also be neglected at very small distances.

In order to estimate  $\alpha_s^{\text{ad}}$  for narrow resonances in the regime of small detuning,  $R^* \ll a$ , we should slightly modify the speculations that lead us to Eq. (36). At distances  $\rho \gg R^*$  the three-body wavefunction behaves practically in the same manner as in the wide resonance case. The deviation is important at distances smaller than  $R^*$ , where, as we have just mentioned, the three-body wavefunction describes a non-interacting atom and a bare molecule. The rate constant reads

$$\alpha_s^{\text{ad}} \sim \left[ \alpha_{s,\text{bare}}^{\text{ad}} \left( \frac{1}{R^*} \right)^3 \right] \times \left[ \left( \frac{R^*}{a} \right)^{2\nu_s+4} a^3 \right], \quad (43)$$

where the first factor is the relaxation rate for an atom and a bare molecule confined to a volume of size  $R^{*3}$  and the second factor is the probability to find three atoms in this volume. We see that the ratio  $\eta_s = \alpha_s^{\text{ad}} / \alpha_{s,\text{bare}}^{\text{ad}}$  interpolates between  $\eta_s \sim (R^*/a)^{2\nu_s+1}$  for small  $R^*/a$  to  $\eta_s = 1$  for large  $R^*/a$ .

The atom-molecule relaxation rate in the  $p$ -wave channel can be estimated in the same fashion. The difference from the  $s$ -wave case is the additional factor  $(ka)^2$ , where  $k$  is the relative atom-molecule momentum. It enters due to the unit angular momentum when we calculate the probability to find the atom and the molecule at distances  $\sim a$ . For the same reason the relaxation rate constant in the

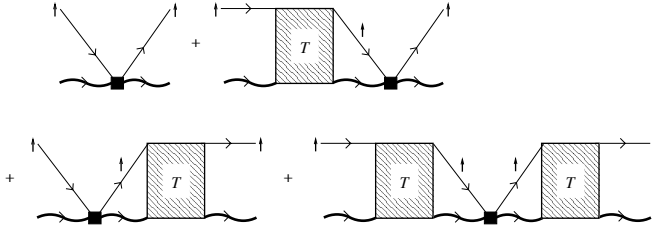


**Fig. 15.** The diagrams leading to the first order corrections to the atom-dimer  $T$ -matrix, Eq. (47).

collision of an atom and a bare molecule is now momentum dependent, i.e.

$$\alpha_{p,\text{bare}}^{\text{ad}}(k) \sim R_e^3 k^2 / m_\downarrow. \quad (44)$$

We also have to take into account the angular momentum when we calculate the relaxation rate of an atom and a bare dimer confined to distances  $R^*$ . It now equals  $\sim \alpha_{p,\text{bare}}^{\text{ad}}(k)/k^2 R^{*5}$ , where we use the fact that  $\alpha_{p,\text{bare}}^{\text{ad}}(k)/k^2$  is momentum independent in the ultracold limit,  $kR_e \ll 1$ . One can show that the ratio  $\eta_p = \alpha_p^{\text{ad}}(k)/\alpha_{p,\text{bare}}^{\text{ad}}(k)$  should behave as  $(R^*/a)^{2\nu_p-1}$  for small  $R^*/a$  and should tend to 1 for large  $R^*/a$ . The power  $\nu_p$  is given by the root of the equation [18]

$$\frac{\nu_p(\nu_p+2)}{\nu_p+1} \cot \frac{\pi \nu_p}{2} + \frac{\nu_p \sin \phi \cos[\phi(\nu_p+1)] - \sin(\nu_p \phi)}{(\nu_p+1) \sin^2 \phi \cos \phi \sin(\pi \nu_p/2)} = 0 \quad (45)$$

in the interval  $-1 < \text{Re } \nu_p < 2$ . For  $m_\uparrow/m_\downarrow = 1$  Eq. (45) gives  $\nu_p \approx 0.773$  and for  $m_\uparrow/m_\downarrow = 6.64$  we get  $\nu_p \approx 0.198$ .

The qualitative analysis of the relaxation rates presented above is valid in the limits of small or large detunings. However, from the practical viewpoint the most interesting is the crossover region,  $R^*/a \sim 1$ . To calculate the inelastic rates in the general case we add to the Hamiltonian (7) a weak imaginary short-range interaction potential between the heavy atoms and bare molecules,

$$H'_{\text{ad}} = -i \sum_{\mathbf{Q}, \mathbf{k}, \mathbf{p}} \frac{\Delta_s^{\text{ad}} + 3\Delta_p^{\text{ad}} \mathbf{k} \cdot \mathbf{p}}{\sqrt{V}} b_{\mathbf{p}}^\dagger a_{\uparrow, \mathbf{Q}-\mathbf{p}}^\dagger b_{\mathbf{k}} a_{\uparrow, \mathbf{Q}-\mathbf{k}}, \quad (46)$$

where the parameters  $\Delta_s^{\text{ad}}$  and  $\Delta_p^{\text{ad}}$  are chosen such that in the extreme limit  $R^*/a \gg 1$  the corresponding relaxation rate constants tend to their bare values  $\alpha_{s,\text{bare}}^{\text{ad}} = 2\Delta_s^{\text{ad}}$  and  $\alpha_{p,\text{bare}}^{\text{ad}}(k) = 6\Delta_p^{\text{ad}} k^2$ .

We can now calculate the ratios  $\eta_s$  and  $\eta_p$  for finite atom-dimer collision energy and for arbitrary  $R^*/a$  by treating Eq. (46) as a perturbation to the Hamiltonian (7). In Fig. 15 we use the unperturbed (elastic)  $T$ -matrix found in Sec. 3 to construct the first order diagrams contributing to the inelastic correction  $\delta T$ . The explicit on-shell expression reads

$$\begin{aligned} \delta T_s(k) &= -i Z \Delta_s^{\text{ad}} \left| \frac{1 + \gamma_s(k)}{1 - i \tan \delta_s(k)} \right|^2 \equiv -i \Delta_s^{\text{ad}} \eta_s(k) \\ \delta T_p(k) &= -i Z \Delta_p^{\text{ad}} k^2 \left| \frac{1 + \gamma_p(k)}{1 - i \tan \delta_p(k)} \right|^2 \equiv -i \Delta_p^{\text{ad}} k^2 \eta_p(k), \end{aligned} \quad (47)$$

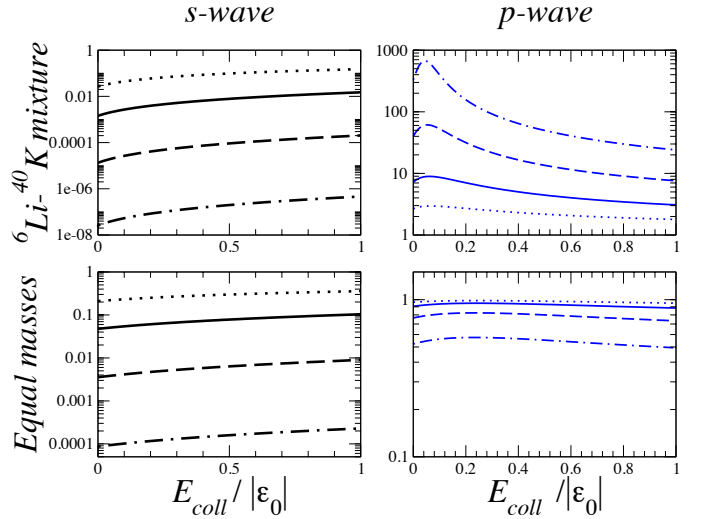


**Fig. 16.** (color online). The ratios  $\eta_s$  (left) and  $\eta_p$  (right) versus collision energy for various detunings:  $R^*/a = 4$  (dotted), 1 (solid),  $1/4$  (dashed), and  $1/16$  (dot-dashed).

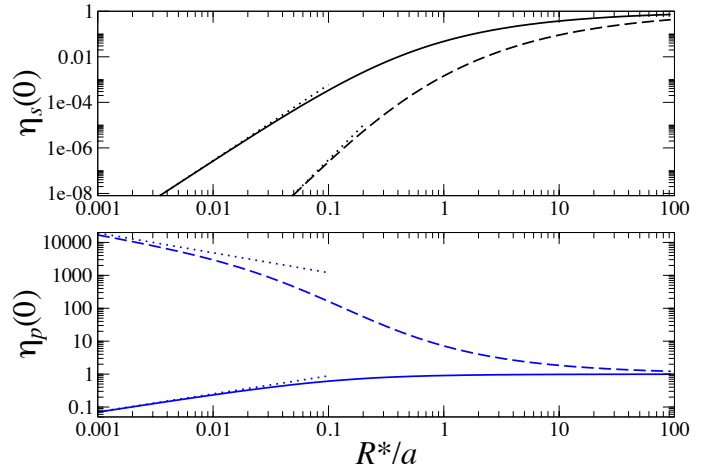


**Fig. 17.** (color online). The ratios  $\eta_s$  (top) and  $\eta_p$  (bottom) at zero collision energy versus  $R^*/a$  for the equal mass case (solid) and the Li-K mixture (dashed). We also show with dotted lines the corresponding power scalings in the limit of small  $R^*/a$  (see text).

where we define

$$\gamma_s(k) = \frac{2}{\pi} \mathcal{P} \int q^2 dq \frac{K_s(k, q)}{q^2 - k^2} \quad (48)$$

$$\gamma_p(k) = \frac{2}{\pi k} \mathcal{P} \int q^3 dq \frac{K_p(k, q)}{q^2 - k^2}. \quad (49)$$

These integrals should be performed by taking the principal value, and  $K_\ell(k, q) = \tilde{f}_\ell(k, q)/[1 + ik\tilde{f}_\ell(k, k)]$  is the solution of Eq. (15) obtained by using the principal value prescription.

Results of our calculation are summarized in Figs. 16 and 17. In Fig. 16 we present the collision energy dependence of  $\eta_s$  and  $\eta_p$ , and Fig. 17 shows their zero energy values versus the detuning  $R^*/a$ . According to their definition these parameters are the suppression or enhancement

factors of the relaxation rate constants  $\alpha_s^{\text{ad}}$  and  $\alpha_p^{\text{ad}}(k)$  compared to their bare values  $\alpha_{s,\text{bare}}^{\text{ad}}$  and  $\alpha_{p,\text{bare}}^{\text{ad}}(k)$ . Note that in the ultracold limit the *s*-wave relaxation is much more dangerous than the *p*-wave one [compare Eqs. (42) and (44)]. Figure 17 thus suggests that the atom-dimer collisions in the heteronuclear case are much less prone to relaxation than in the homonuclear one. Indeed, in the Li-K case already for  $R^*/a = 1$  the *s*-wave relaxation is suppressed by three orders of magnitude. We think that this is promising for the system's longevity even though the *p*-wave relaxation for this  $R^*/a$  is enhanced by an order of magnitude. At this point we can also make the following observation: in order to suppress collisional relaxation in the homonuclear case one should make the detuning as small as possible, whereas in the Li-K case there exists an optimal detuning where the inelastic atom-dimer collisional losses reach their minimum. The exact value of such optimal detuning depends on the average momentum  $k$  and on the actual values of the bare relaxation rates  $\alpha_{s,\text{bare}}^{\text{ad}}$  and  $\alpha_{p,\text{bare}}^{\text{ad}}(k)$ .

### 5.1 Relaxation in dimer-dimer collisions

The dimer-dimer scattering problem is more complicated than the atom-dimer one in many respects. In particular, one has to deal not only with the relaxation channel which requires two heavy and one light fermion to approach each other to short distances but also with analogous processes in the heavy-light-light subsystem. In fact, in the regime of intermediate detuning ( $R^*/a \gg 1$ ) the occupation of the bare molecular states is dominant, and the above mentioned “three-body” channels are suppressed as they require one of the atoms to be in the open channel. Then the dominant decay scenario is the relaxation in collisions of bare molecules. In this case the perturbation is

$$H'_{\text{dd}} = -i \sum_{\mathbf{Q}, \mathbf{k}, \mathbf{p}} \frac{\Delta_s^{\text{dd}}}{\sqrt{V}} b_{\mathbf{p}}^\dagger b_{\mathbf{Q}-\mathbf{p}}^\dagger b_{\mathbf{k}} b_{\mathbf{Q}-\mathbf{k}}, \quad (50)$$

and we treat it in the same fashion as (46). Equation (50) correctly describes the relaxation in the limit  $R^*/a \gg 1$  if we set  $\Delta_s^{\text{dd}} = \alpha_{\text{bare}}^{\text{dd}}/4$ . The diagrams leading to the lowest order correction to the dimer-dimer *T*-matrix are depicted in Fig. 18. The on-shell  $\delta T$  at vanishing collision energy equals

$$\begin{aligned} \delta T(0) &= -2iZ^2 \Delta_s^{\text{dd}} \left| 1 + \frac{i}{g^4 Z^2} \int \frac{d^4 q}{(2\pi)^4} D(\mathbf{q}, \epsilon_0 + q_0) \right. \\ &\quad \times D(-\mathbf{q}, \epsilon_0 - q_0) T(q, q_0) \Big|^2 \\ &\equiv -2i \Delta_s^{\text{dd}} \eta_s^{\text{dd}}, \end{aligned} \quad (51)$$

where  $T(q, q_0)$  is the solution of the dimer-dimer integral equation (28), and  $\eta_s^{\text{dd}}$  is the ratio of the actual relaxation rate constant at a given  $R^*/a$  to its bare value (at  $R^*/a = \infty$ ). This parameter is plotted in Fig. 19 versus the detuning  $R^*/a$  and we see that this “four-atom” relaxation mechanism is suppressed for small detunings. The

power law dependence in this limit can be understood in a similar fashion as in the atom-dimer case. We start with two molecules in a unit volume. The probability to find them within the distance  $\sim a$  equals  $a^3$ . Then, at shorter distances the four-body wavefunction is proportional to  $\rho^{\nu_{\text{4body}}-1}$ , where  $\rho$  is the four-body hyperradius. Thus, given that the four atoms are confined to the volume  $\sim a^3$ , the probability to find them at hyperradii  $\rho \lesssim R^*$  equals  $(R^*/a)^{2\nu_{\text{4body}}+7}$ , where we take into account that the four-body configurational volume in the center-of-mass frame scales as  $\rho^9$ . At hyperradii  $\rho \lesssim R^*$  we deal with two bare molecules and the relaxation rate is given by  $\alpha_{\text{bare}}^{\text{dd}}/R^{*3}$ . Finally, for the dimer-dimer relaxation rate constant associated with the “four atom” relaxation mechanism in the limit  $R^*/a \ll 1$  we obtain

$$\alpha^{\text{dd}} = \alpha_{\text{bare}}^{\text{dd}} (R^*/a)^{2\nu_{\text{4body}}+4}. \quad (52)$$

The power  $\nu_{\text{4body}}$  may be obtained by calculating the ground state energy of the four-body system in the unitarity limit in a harmonic potential which has been carried out in Ref. [47] for various mass ratios. We cite the following results [47]:  $\nu_{\text{4body}} \approx 0.0$  for  $m_\uparrow/m_\downarrow = 1$ ,  $\nu_{\text{4body}} \approx 0.3$  for  $m_\uparrow/m_\downarrow = 4$ , and  $\nu_{\text{4body}} \approx 0.5$  for  $m_\uparrow/m_\downarrow = 8$ . Our numerical calculations for the dimer-dimer relaxation in the limit  $R^*/a \ll 1$  are consistent with Eq. (52) with these powers.

Figure 19 only shows the result corresponding to the “four-body” mechanism of dimer-dimer relaxation (dominant at intermediate detunings) and thus presents a lower bound for the relaxation rate constant. We see that for  $R^*/a \sim 1$  the dimer-dimer relaxation is less suppressed compared to the atom-dimer case. Consequently, this region of detunings is more suitable for studies of atom-dimer mixtures with low concentration of molecules. Otherwise, if one wants to study mixtures with higher molecular concentrations, it is necessary to decrease the detuning as much as possible.

In the regime of small detuning the “three-body” mechanisms of dimer-dimer relaxation can be as important as the “four-body” one. For wide resonances the “three-body” cases are described in detail in Ref. [17, 36]. These results can be easily generalized to the regime of small detunings near a narrow resonance by counting probabilities as we did earlier in this section in order to estimate the atom-dimer relaxation rates. Let us present the final results. The dimer-dimer relaxation rate constant originating from the *s*-wave atom-dimer relaxation mechanism equals (up to a numerical prefactor) the one for the atom-dimer collisions given by Eq. (43). Namely,

$$\alpha_{s-\text{ad}}^{\text{dd}} \sim \alpha_{s,\text{bare}}^{\text{ad}} (R^*/a)^{2\nu_s+1}. \quad (53)$$

The dimer-dimer relaxation rate constant originating from the *p*-wave atom-dimer relaxation mechanism equals

$$\begin{aligned} \alpha_{p-\text{ad}}^{\text{dd}} &\sim \alpha_{p,\text{bare}}^{\text{ad}} (1/a) (R^*/a)^{2\nu_p-1} \\ &\sim (R_e^3/m_\downarrow a^2) (R^*/a)^{2\nu_p-1}. \end{aligned} \quad (54)$$

Equations (53) and (54) can be modified to describe the light-light-heavy relaxation mechanism. In this case the

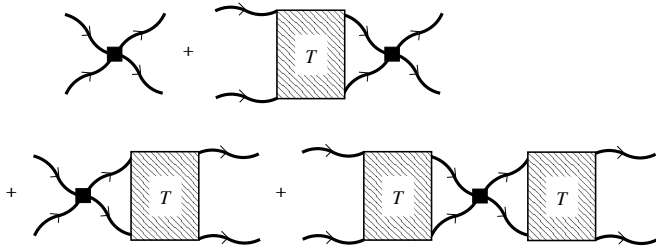


**Fig. 18.** The diagrams leading to the first order correction to the dimer-dimer  $T$ -matrix, Eq. (51).

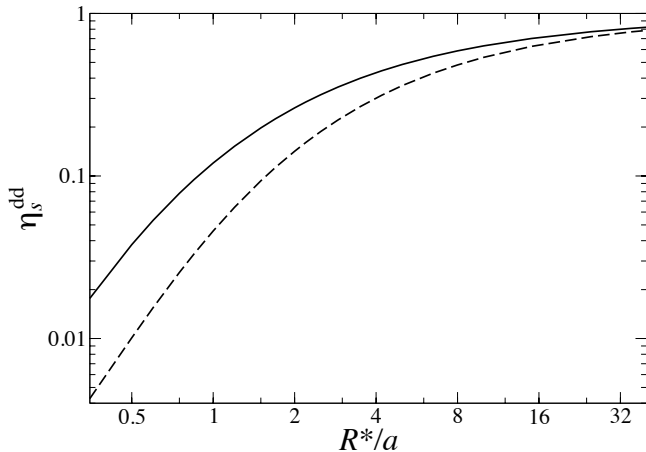


**Fig. 19.** The relaxation rate in dimer-dimer collisions.

bare rates  $\alpha_{s,\text{bare}}^{\text{ad}}$  and  $\alpha_{p,\text{bare}}^{\text{ad}}(k)$  should be taken for the collisions of light atoms and bare molecules, and the powers  $\nu_s$  and  $\nu_p$  should correspond to the light-light-heavy three-body system with zero and unit angular momenta respectively. For  $m_\uparrow/m_\downarrow = m_K/m_{\text{Li}}$  they equal  $\nu_s \approx 1.01$  and  $\nu_p \approx 0.945$ .

## 6 Concluding remarks

Concluding the paper, we would like to discuss several issues, which, from our viewpoint, are important for future studies. We believe that the  $p$ -wave atom-dimer resonance should significantly influence the behavior of a mixture of weakly bound K-Li molecules and K atoms. The “simplest” many-body problem in which the effect of the resonance should be visible is the problem of a single atom immersed in a BEC of molecules or a single molecule immersed in a Fermi sea of atoms. Let us consider, for example, the former case. In the limit  $v_{\text{ad}}n \ll 1$ , where  $n$  is the BEC density, we compute the correction to the dispersion curve of the polaron due to the  $p$ -wave interaction with molecules. By using the standard diagrammatic techniques, the dispersion is found to be

$$\epsilon_K(q) \simeq \frac{q^2}{2m_\uparrow} + \frac{3\pi n v_{\text{ad}} q^2}{2\mu_3}. \quad (55)$$

We see that in the case of a negative and large  $p$ -wave scattering volume  $v_{\text{ad}}$ , the effective mass of the polaron

increases, which can be measured in an experiment similar to the one performed recently at ENS on collective modes of a homonuclear  ${}^6\text{Li}$  spin-mixture [48]. Most interesting seems to be the regime  $|v_{\text{ad}}|n \sim 1$ , where the validity of the mean-field approach is not guaranteed even on the qualitative level and a non-perturbative analysis is required. Our few-body results suggest that the crossover phase diagram in the K-Li case should be less “mean-field friendly” than the one in the homonuclear case. The same holds for the case of a single heavy-light molecule immersed in a Fermi sea of the heavy species. Variational analysis [49] suggests that such molecules can form a BEC with finite momentum (an analog of the FFLO phase). In a related work [50], it was demonstrated that the phase diagram of a two-species bosonic mixture near a  $p$ -wave interspecies Feshbach resonance is quite rich and features, in particular, a finite-momentum superfluid phase.

In this paper we have shown that the atom-dimer scattering is characterized by a very strong dependence on the angular momentum, the effect being remarkably pronounced for the K-Li mass ratio. To observe the interference between the  $s$ - and  $p$ -waves we have proposed a scattering experiment in which one collides a cloud of atoms with a cloud of molecules. Depending on the collision energy the scattering goes predominantly in the forward or backward directions. The contrast in this experiment is limited to approximately 75% due to the fact that only two partial waves are involved. We believe that a similar experiment in a quasi-1D geometry would show a complete destructive or constructive interference, i.e. transmissionless or reflectionless 1D scattering at certain values of the collision energy. The control over the atom-dimer scattering properties provided by the external quasi-1D confinement opens up interesting perspectives for observing rather exotic effects. For example, in the case of a vanishing transmission coefficient the propagation of a molecule immersed in a quasi-1D gas of heavy fermions is suppressed, leading to degeneracies in its excitation spectrum and an unusual dynamical correlation function [51]. Besides, as in the quasi-2D case [20], the quasi-1D confinement can push the trimer state below the atom-dimer threshold, i.e. make it bound. The quasi-1D confinement of only one of the species leads to similar effects and can be used to control the atom-dimer scattering amplitude [52, 53].

In the present paper we focus on the  ${}^6\text{Li}-{}^{40}\text{K}$  mixture in which the Feshbach molecule is bosonic and the enhanced  $p$ -wave interaction occurs between a boson and a fermion. On the other hand, our approach applies equally well to the case of light bosonic atoms. If, for example, the light particle is chosen to be  ${}^7\text{Li}$ , the enhanced interaction takes place between a fermionic atom and a fermionic dimer. In this case, however, relaxation in molecule-molecule collisions is not suppressed by the Pauli exclusion principle as two bosons and one fermion can easily approach each other. Nevertheless, the fact that the molecules are identical fermions is advantageous for the system’s longevity. Such a mixture of fermionic atoms and molecules can be

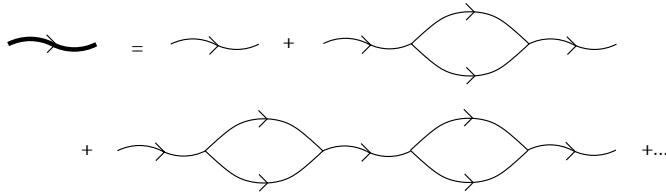


**Fig. 20.** The propagator of dimers consists of an admixture of closed channel Feshbach molecules (thin wave lines) and open channel fermionic loops.

seriously considered for studies of the BCS-BEC crossover with resonant  $p$ -wave interspecies interactions.

We acknowledge support by the EuroQUAM-FerMix program, by the IFRAF Institute, and by the Russian Foundation for Fundamental Research. One of us (J.L.) acknowledges support by a Marie Curie Intra European Fellowship within the 7th European Community Framework Programme. LPTMS is a mixed research unit No. 8626 of CNRS and Université Paris Sud.

## A Two-body scattering amplitude and propagator of dimers

In this appendix we obtain the dressed dimer propagator and relate the bare parameters of the Hamiltonian, Eq. (7), to the physical observables of the scattering process between a heavy and a light fermionic atom. The propagator of the bare (closed-channel) molecule is

$$D_0(\mathbf{p}, p_0) = \frac{1}{p_0 - p^2/2M - \omega_0 + i0}. \quad (56)$$

The dressed propagator is obtained by resumming the diagrams of Fig. 20, resulting in

$$D(\mathbf{p}, p_0) = \frac{g^2}{D_0^{-1}(\mathbf{p}, p_0) - g^2 \Pi(\mathbf{p}, p_0)}. \quad (57)$$

The fermion loop  $\Pi$  is

$$\Pi(\mathbf{p}, p_0) \equiv i \int \frac{d^4 Q}{(2\pi)^4} G_\uparrow(p+Q) G_\downarrow(-Q) \quad (58)$$

$$= -\frac{\mu\Lambda}{\pi^2} + \frac{\mu^{3/2}}{\sqrt{2\pi}} \sqrt{-p_0 + p^2/2M - i0}. \quad (59)$$

The cut-off at large momenta,  $\Lambda$ , is the inverse van der Waals range of the potential. We have chosen to include an extra factor  $g^2$  in the dressed dimer propagator. This is purely for bookkeeping purposes, as this propagator always appears along with a factor of  $g^2$  in Feynman diagrams, providing an easy manner of keeping tracks of powers of the coupling constant. The dressed propagator is

$$D(\mathbf{p}, p_0) = g^2 \left[ p_0 - \frac{p^2}{2M} - \omega_0 + \frac{g^2 \mu \Lambda}{\pi^2} \right]$$

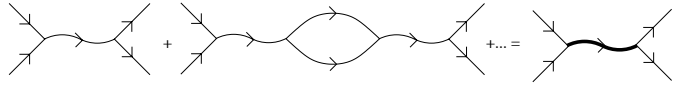


**Fig. 21.** The relationship between the scattering amplitude for elastic heavy-light atom scattering and the dressed dimer propagator.

$$-\frac{g^2 \mu^{3/2}}{\sqrt{2\pi}} \sqrt{-p_0 + \frac{p^2}{2M} - i0} \Big]^{-1}. \quad (60)$$

Let us now relate the bare parameters,  $g$  and  $\omega_0$ , to the physical parameters  $a$  and  $R^*$  of Eq. (3). To this end we calculate the amplitude of elastic heavy-light atom scattering in the model Eq. (7). Let the heavy atom have four-momentum  $(\mathbf{k}, k^2/2m_\uparrow)$  and the light have  $(-\mathbf{k}, k^2/2m_\downarrow)$ . The scattering is depicted in Fig. 21. The summation of diagrams takes the same form as above, Eq. (58), and recalling that  $g^2$  has been absorbed into the dimer propagator, the scattering amplitude is

$$\begin{aligned} T_2(\mathbf{k}, -\mathbf{k}) &= D(\mathbf{0}, k^2/2\mu) \\ &= \frac{2\pi}{\mu} \frac{1}{\frac{2\pi}{\mu g^2} \left( -\omega_0 + \frac{g^2 \mu \Lambda}{\pi^2} \right) + \frac{\pi}{\mu^2 g^2} k^2 + ik}. \end{aligned} \quad (61)$$

Comparing with the scattering amplitude at low momenta,  $k \lesssim a^{-1}$ ,

$$T_2(\mathbf{k}, -\mathbf{k}) \equiv -\frac{2\pi}{\mu} f(\mathbf{k}, -\mathbf{k}) \approx \frac{2\pi}{\mu} \frac{1}{a^{-1} + R^* k^2 + ik} \quad (62)$$

the scattering length and effective range are found to be

$$a = \frac{\mu g^2}{2\pi} \frac{1}{\frac{g^2 \mu \Lambda}{\pi^2} - \omega_0}, \quad R^* = \frac{\pi}{\mu^2 g^2}. \quad (63)$$

In terms of the physical observables, the dimer propagator (60) then takes the form (10).

The binding energy of the heteronuclear molecule is found as the energy pole of the propagator and is

$$\epsilon_0 = -\frac{\left[ \sqrt{1 + 4R^*/a} - 1 \right]^2}{8\mu R^{*2}}. \quad (64)$$

Since  $R^* \geq 0$  there is only one such pole on the physical sheet. The residue at the energy pole is needed for proper renormalization of the three- and four-body T-matrices, and is

$$g^2 Z = \frac{\pi}{\mu^2 R^*} \left( 1 - \frac{1}{\sqrt{1 + 4R^*/a}} \right). \quad (65)$$

Each external dimer propagator acquires a factor  $\sqrt{Z}$  in the few-body scattering problems.

## B The kernel of the 4-body integral equation

$\Gamma^{(0)}$  is the result of calculating the Born diagram,

$$\begin{aligned} \Gamma^{(0)}(q, q_0; p, p_0) = & \\ -i \int \frac{d\Omega_q}{4\pi} \int \frac{d^4 Q}{(2\pi)^4} G_{\uparrow} \left( \mathbf{Q} + \frac{\mathbf{p}}{2} + \frac{\mathbf{q}}{2}, \frac{\epsilon_0}{2} + Q_0 + \frac{p_0}{2} + \frac{q_0}{2} \right) & \\ \times G_{\uparrow} \left( \mathbf{Q} - \frac{\mathbf{p}}{2} - \frac{\mathbf{q}}{2}, \frac{\epsilon_0}{2} + Q_0 - \frac{p_0}{2} - \frac{q_0}{2} \right) & \\ \times G_{\downarrow} \left( -\mathbf{Q} - \frac{\mathbf{p}}{2} + \frac{\mathbf{q}}{2}, \frac{\epsilon_0}{2} - Q_0 - \frac{p_0}{2} + \frac{q_0}{2} \right) & \\ \times G_{\downarrow} \left( -\mathbf{Q} + \frac{\mathbf{p}}{2} - \frac{\mathbf{q}}{2}, \frac{\epsilon_0}{2} - Q_0 + \frac{p_0}{2} - \frac{q_0}{2} \right) & \\ = -2 \int \frac{d\Omega_q}{4\pi} \int \frac{d^3 Q}{(2\pi)^3} \frac{A}{(A^2 - B^2)(A^2 - C^2)}, & (66) \end{aligned}$$

with

$$\begin{aligned} A &= \epsilon_0 - \frac{Q^2}{2\mu} - \frac{p^2}{8\mu} - \frac{q^2}{8\mu} - \frac{\mathbf{p} \cdot \mathbf{q}}{4m_{\uparrow}} + \frac{\mathbf{p} \cdot \mathbf{q}}{4m_{\downarrow}}, \\ B &= p_0 - \frac{\mathbf{Q} \cdot \mathbf{p}}{2m_{\uparrow}} + \frac{\mathbf{Q} \cdot \mathbf{p}}{2m_{\downarrow}} - \frac{\mathbf{Q} \cdot \mathbf{q}}{2\mu}, \\ C &= q_0 - \frac{\mathbf{Q} \cdot \mathbf{q}}{2m_{\uparrow}} + \frac{\mathbf{Q} \cdot \mathbf{q}}{2m_{\downarrow}} - \frac{\mathbf{Q} \cdot \mathbf{p}}{2\mu}. \end{aligned} \quad (67)$$

## References

1. M. Inguscio, W. Ketterle, C. Salomon, eds., *Ultracold Fermi Gases, Proceedings of the International School of Physics "Enrico Fermi"*, (IOS Press, Amsterdam 2008)
2. S. Giorgini, L.P. Pitaevskii, S. Stringari, Rev. Mod. Phys. **80**, 1215 (2008)
3. M. Taglieber, A.-C. Voigt, T. Aoki, T.W. Hänsch, K. Dieckmann, Phys. Rev. Lett., **100**, 010401 (2008)
4. E. Wille, F.M. Spiegelhalder, G. Kerner, D. Naik, A. Trenkwalder, G. Hendl, F. Schreck, R. Grimm, T.G. Tiecke, J.T.M. Walraven, S.J.J.M.F. Kokkelmans, E. Tiesinga, P.S. Julienne, Phys. Rev. Lett. **100**, 053201 (2008)
5. A.-C. Voigt, M. Taglieber, L. Costa, T. Aoki, W. Wieser, T.W. Hänsch, K. Dieckmann, Phys. Rev. Lett. **102**, 020405 (2009)
6. F.M. Spiegelhalder, A. Trenkwalder, D. Naik, G. Hendl, F. Schreck, R. Grimm, Phys. Rev. Lett. **103**, 223203 (2009)
7. T.G. Tiecke, M.R. Goosen, A. Ludewig, S.D. Gensemer, S. Kraft, S.J.J.M.F. Kokkelmans, J.T.M. Walraven, Phys. Rev. Lett. **104**, 053202 (2010)
8. F.M. Spiegelhalder, A. Trenkwalder, D. Naik, G. Kerner, E. Wille, G. Hendl, F. Schreck, R. Grimm, Phys. Rev. A **81**, 043637 (2010)
9. L. Costa, H. Brachmann, A.-C. Voigt, C. Hahn, M. Taglieber, T. W. Hnsch, K. Dieckmann, Phys. Rev. Lett. **105**, 123201 (2010)
10. A. Trenkwalder, C. Kohstall, M. Zaccanti, D. Naik, A.I. Sidorov, F. Schreck, R. Grimm, arXiv:1011.5192v1 (2010)
11. A species selective optical lattice can be applied to modify the effective mass ratio.
12. D.S. Petrov, G.E. Astrakharchik, D.J. Papoular, C. Salomon, G.V. Shlyapnikov, Phys. Rev. Lett. **99**, 130407 (2007)
13. L.D. Landau, E.M. Lifshitz, *Quantum Mechanics*, (Butterworth-Heinemann, Oxford 1981)
14. V.N. Efimov, Nucl. Phys. A **210**, 157 (1973)
15. A.C. Fonseca, E.F. Redish, P.E. Shanley, Nucl. Phys. A. **320**, 273 (1979)
16. R.D. Amado, J.V. Noble, Phys. Lett. **35B**, 25 (1971)
17. D.S. Petrov, C. Salomon, G.V. Shlyapnikov, J. Phys B: At. Mol. Opt. Phys. **38**, S645 (2005)
18. D.S. Petrov, Phys. Rev. A **67**, 010703(R) (2003)
19. O.I. Kartavtsev, A.V. Malykh, J. Phys. B **40**, 1429 (2007)
20. J. Levinsen, T.G. Tiecke, J.T.M. Walraven, D.S. Petrov, Phys. Rev. Lett. **103**, 153202 (2009)
21. We note that in a many-body problem, the width of the resonance can be characterized by comparing  $|r_0|$  with the mean interparticle separation. In particular, the narrow resonance condition  $(n|r_0|^3)^{-1/3} \ll 1$  (much more strict than  $|r_0| \gg R_e$ ) allows for a perturbative expansion across the whole BCS-BEC crossover [23].
22. D.S. Petrov, Phys. Rev. Lett. **93**, 143201 (2004)
23. V. Gurarie, L. Radzhovsky, Ann. Phys. **322**, 2 (2007)
24. In principle, the method that we develop in this paper can be generalized to an arbitrary energy dependence of the phase shift.
25. E. Timmermans, P. Tommasini, M. Hussein, A. Kerman Physics Reports **315**, 199 (1999)
26. G.V. Skorniakov, K.A. Ter-Martirosian, Zh. Eksp. Teor. Phys. **31**, 775 (1956), [Sov. Phys. JETP **4**, 648 (1957)]
27. P.F. Bedaque, H.-W. Hammer, U. van Kolck, Phys. Rev. C **58**, R641 (1998)
28. M. Born, J.R. Oppenheimer, Ann. der Phys. **84**, 457 (1927)
29. H. Bethe, R. Peierls, Proc. R. Soc. London **A148**, 146, (1935)
30. Quantum interference of *s*- and *d*-waves has been observed in collisions of <sup>87</sup>Rb BECs at rather high collision energies, see Ch. Buggle, J. Léonard, W. von Klitzing, J.T.M. Walraven, Phys. Rev. Lett. **93**, 173202 (2004); N.R. Thomas, N. Kjærgaard, P.S. Julienne, A.C. Wilson, Phys. Rev. Lett. **93**, 173201 (2004)
31. J. Levinsen, V. Gurarie, Phys. Rev. A **73**, 053607 (2006)
32. D.S. Petrov, C. Salomon, G.V. Shlyapnikov Phys. Rev. Lett. **93**, 090404 (2004)
33. I.V. Brodsky, A.V. Klaptsov, M.Yu. Kagan, R. Combescot, X. Leyronas JETP Lett. **82**, 273 (2005)
34. G.E. Astrakharchik, J. Boronat, J. Casulleras, S. Giorgini, Phys. Rev. Lett. **93**, 200404 (2004)
35. J. von Stecher, C.H. Greene, D. Blume, Phys. Rev. A **76**, 053613 (2007)
36. D.S. Petrov, C. Salomon, G.V. Shlyapnikov, Phys. Rev. A **71**, 012708 (2005)
37. J. Levinsen, Ph.D. thesis, University of Colorado at Boulder (2007), arXiv:0807.2840v1
38. B. Marcelis, S.J.J.M.F. Kokkelmans, G.V. Shlyapnikov, D.S. Petrov, Phys. Rev. A **77**, 032707 (2008)
39. D. Blume, private communication
40. The second term in Eq. (34) can be cast in the form of an integral. Its analytic integration is not possible, but numerically the result can be obtained with a very well controlled accuracy.
41. V.N. Efimov, Yad. Fiz. **12**, 1080 (1970) [Sov. J. Nucl. Phys. **12**, 589 (1971)]
42. E. Nielsen, D.V. Fedorov, A.S. Jensen, E. Garrido, Phys. Rep. **347**, 373 (2001)
43. E. Braaten, H.-W. Hammer, Annals Phys. **322**, 120 (2007)

44. J.P. D'Incao, B.D. Esry, Phys. Rev. Lett. **94**, 213201 (2005)
45. In Ref. [46] the atom-dimer relaxation in *s*-wave collisions in the case  $m_\uparrow = m_\downarrow$  is considered by using a different method. Equation (42) disagrees with the power law stated in that article. We think that the authors do not reach sufficiently large values of  $R^*/a$ .
46. Y. Wang, J.P. D'Incao, B.D. Esry, arXiv:0906.5019 (2009)
47. J. von Stecher, C. H. Greene, D. Blume, Phys. Rev. A **77**, 043619 (2008)
48. S. Nascimbene, N. Navon, K. Jiang, L. Tarruell, M. Teichmann, J. McKeever, F. Chevy, C. Salomon, Phys. Rev. Lett. **103**, 170402 (2009)
49. C.J.M. Mathy, M.M. Parish, D.A. Huse, arxiv:1002.0101 (2010)
50. L. Radzihovsky, S. Choi, Phys. Rev. Lett. **103**, 095302 (2009)
51. M.B. Zvonarev, V.V. Cheianov, T. Giamarchi, Phys. Rev. Lett. **99**, 240404 (2007)
52. Y. Nishida, S. Tan, Phys. Rev. Lett. **101**, 170401 (2008)
53. Y. Nishida, S. Tan, Phys. Rev. A **79**, 060701(R) (2009)